AD_____

Award Number: W81XWH-06-1-0462

TITLE: Optimization and Comparison of Different Digital Mammographic Tomosynthesis Reconstruction Methods

PRINCIPAL INVESTIGATOR: Ying Chen, M.S.
James T. Dobbins III, Ph.D.

CONTRACTING ORGANIZATION: Duke University
Durham, North Carolina, 27710

REPORT DATE: April 2007

TYPE OF REPORT: Annual Summary

PREPARED FOR: U.S. Army Medical Research and Materiel Command
Fort Detrick, Maryland 21702-5012

DISTRIBUTION STATEMENT: Approved for Public Release;
Distribution Unlimited

The views, opinions and/or findings contained in this report are those of the author(s) and should not be construed as an official Department of the Army position, policy or decision unless so designated by other documentation.

REPORT DOCUMENTATION PAGE

Form Approved
OMB No. 0704-0188

Public reporting burden for this collection of information is estimated to average 1 hour per response, including the time for reviewing instructions, searching existing data sources, gathering and maintaining the data needed, and completing and reviewing this collection of information. Send comments regarding this burden estimate or any other aspect of this collection of information, including suggestions for reducing this burden to Department of Defense, Washington Headquarters Services, Directorate for Information Operations and Reports (0704-0188), 1215 Jefferson Davis Highway, Suite 1204, Arlington, VA 22202-4302. Respondents should be aware that notwithstanding any other provision of law, no person shall be subject to any penalty for failing to comply with a collection of information if it does not display a currently valid OMB control number. **PLEASE DO NOT RETURN YOUR FORM TO THE ABOVE ADDRESS.**

1. REPORT DATE *(DD-MM-YYYY)*	**2. REPORT TYPE**	**3. DATES COVERED** *(From - To)*
01/04/07	Annual Summary	1 Apr 2006 – 31 Mar 2007

4. TITLE AND SUBTITLE

Optimization and Comparison of Different Digital Mammographic Tomosynthesis Reconstruction Methods

5a. CONTRACT NUMBER

5b. GRANT NUMBER
W81XWH-06-1-0462

5c. PROGRAM ELEMENT NUMBER

6. AUTHOR(S)
Ying Chen, M.S. and James T. Dobbins III, Ph.D.

E-Mail: adachen@duke.edu

5d. PROJECT NUMBER

5e. TASK NUMBER

5f. WORK UNIT NUMBER

7. PERFORMING ORGANIZATION NAME(S) AND ADDRESS(ES)

Duke University
Durham, North Carolina, 27710

8. PERFORMING ORGANIZATION REPORT NUMBER

9. SPONSORING / MONITORING AGENCY NAME(S) AND ADDRESS(ES)
U.S. Army Medical Research and Materiel Command
Fort Detrick, Maryland 21702-5012

10. SPONSOR/MONITOR'S ACRONYM(S)

11. SPONSOR/MONITOR'S REPORT NUMBER(S)

12. DISTRIBUTION / AVAILABILITY STATEMENT
Approved for Public Release; Distribution Unlimited

13. SUPPLEMENTARY NOTES

14. ABSTRACT: **Digital breast tomosynthesis is a three dimensional imaging technique with limited angle series of projection images that allows the reconstruction of an arbitrary set of planes in the breast. Compared with standard mammography techniques, this method improves conspicuity of structures by removing the visual clutter associated with overlying anatomy. The objective of this project is to optimized and compare different tomosynthesis methods and choose the optimal one for breast imaging. Optimization of acquisition parameters will provide better reconstruction images of the breast, and related deblurring methods can remove out of plane blurred structures. We investigated several 3D tomosynthesis reconstruction algorithms and studied the effect of acquisition parameters for different reconstruction algorithms, according to physical measurements of impulse response analysis, modulation transfer function (MTF) and noise power spectrum.**

15. SUBJECT TERMS
Mammography, tomosynthesis, noise power spectrum, modulation transfer function, shift-add-add(SAA), filtered back projection (FPB), matrix inversion tomosynthesis (MITS), maximum likelihood expectation maximization (MLEM)

16. SECURITY CLASSIFICATION OF:			**17. LIMITATION OF ABSTRACT**	**18. NUMBER OF PAGES**	**19a. NAME OF RESPONSIBLE PERSON**
a. REPORT	**b. ABSTRACT**	**c. THIS PAGE**			USAMRMC
U	U	U	UU	60	**19b. TELEPHONE NUMBER** *(include area code)*

Table of Contents

INTRODUCTION

Breast cancer has been considered as a major problem and the most common cancer among women. Annually, a total of 348,000 cases of breast cancer is diagnosed and almost 115,000 are killed by this in the US and European Community [1]. Tremendous efforts have been made in the incremental improvements in imaging technologies in the field of breast cancer detection. Mammography is currently the most important and efficacious tool for the early detection of breast cancer [2]. However, the nature of the two-dimensional mammography makes it very difficult to distinguish a cancer from overlying breast tissues, especially for dense breast cases.

Digital breast tomosynthesis is a three-dimensional breast imaging method that allows the reconstruction of an arbitrary set of planes in the breast from limited-angle series of projection images as the x-ray source moves along an arc above the breast. A variety of tomosynthesis reconstruction algorithms have been proposed including the traditional shift-and-add (SAA), the image-stretching method proposed by Nilklason and colleagues [3], the maximum likelihood iterative algorithm (MLEM) by Wu et al. [4,5], tuned-aperture computed tomography (TACT) reconstruction methods developed by Webber and investigated by Suryanarayanan *et al* [6,7], algebraic reconstruction techniques (ART) [8,9,10], filtered back projection (FBP) [11,12,13], and matrix inversion tomosynthesis (MITS) [14,15].

The purpose of this project is to optimize and compare several different tomosynthesis reconstruction algorithms that are either initially investigated in our lab or currently very popular, and to optimize the imaging acquisition techniques. Based on this project, we hope to contribute to the optimal breast tomosynthesis technique for better breast cancer detection.

BODY

Task 1. Optimization of different candidate tomosynthesis reconstruction methods (Month 1-12):

1.1. Select candidate algorithms from different algorithm families for optimization and comparison. 2-4 candidate algorithms from different algorithm families will be chosen. (Month 1-4).

We have investigated a few reconstruction algorithms, including shift-and-add (SAA) algorithm, Nilklason's image stretching shift-and-add (NIKL), maximum likelihood expectation maximization (MLEM), matrix inversion tomosynthesis (MITS), and filtered back projection (FBP).

We found that the traditional shift-and-add (SAA) is a common mathematical method to line up each projection image based on its shifting amount to generate reconstruction slices. MITS was originally invented in our lab by Dobbins [15] and we applied it to the breast tomosynthesis imaging successfully [14]. MITS shows better high frequency response in removing out-of-plane blur. We also developed our FBP reconstruction based on central slice theorem and Fourier frequency sampling density. In order to control the high frequency noise amplification, Hamming Gaussian filters were designed and applied to our FBP algorithm [12]. MLEM algorithm is an effective iterative method in breast tomosynthesis reconstruction. However, it is time-consuming due to intensive computation. Therefore, in this project, we selected SAA, MITS and FBP as our three candidate algorithms for comparison and optimization. But we also

did related research on other algorithms such as point-by-point back projection (BP), NIKL, and MLEM.

Work for this specific task also resulted in part of a manuscript that we submitted to the journal of Medical Physics for publication (reportable outcome #1). During our investigation of different algorithms, we found that quite a few other algorithms depend on a traditional SAA method. However, traditional SAA is not appropriate for the isocentric motion in digital breast tomosynthesis because it doesn't take into the account of shift amount at the direction orthogonal to tube's motion direction. A simple SAA reconstruction algorithm is not entirely suitable for breast tomosynthesis, especially for small structures such as microcalcifications, which have an important bearing in clinical breast cancer detection tasks. The manuscript we submitted focused on the importance of point-by-point back projection for reconstruction of small structures such as microcalcifications.

1.2. Characterize the effect of three acquisition parameters including total Tomographic-Angle (TA), Number of projection images (N), and Reconstruction-Slice-Spacing (RSS) for each reconstruction algorithm, according to physical measurements of impulse response analysis, modulation transfer function (MTF) and noise power spectrum (NPS). (Months 5-12).

1.2.1. Simulate impulses with different acquisition parameters. Apply each candidate tomosynthesis algorithms to generate slice reconstruction images. Analyze the impulse response of each candidate algorithm. (Months 5-7)
Work on this task began well ahead of schedule during the first year. We simulated impulses by ray-tracing method with a few different combinations of acquisition parameters. The candidate tomosynthesis algorithms were used to generate slice reconstruction images. The impulse response of each candidate algorithm was analyzed.

Parameters of a selenium-based direct conversion Siemens Mammomat Novation DR prototype system was modified to be used for geometries of the simulation. Two different impulse locations were investigated in the project: 1) an impulse that is exactly underneath the x-ray source (near the chest wall) and in a defined reconstructed plane (20 mm above the detector surface); 2) an impulse that is approximately 4 cm away from the chest wall and in a defined reconstructed plane (20 mm above the detector surface). Datasets of the impulse with different number of projections images N and total Tomographic Angle TA of the simulated x-ray point source were simulated and reconstructed by each candidate algorithm for comparison.

We found that the shift-and-add method (SAA) was similar to the Niklason method (NIKL) in all cases examined. Compared with SAA and NIKL methods, MITS and FBP were always better for removal of out-of-plane blur artifacts. For optimization of Number of projection images (N), not much difference was noted between cases with different N for comparison of SAA. For MITS and FBP, bigger N cases were better in high frequency noise removal.

Figure 1 shows an example of our investigation to optimize the N parameter when the impulse was located exactly underneath the x-ray tube and halfway between two neighboring planes, which are represented by Z-0.5mm and Z+0.5mm. In this simulation, Z=19.5mm above the

detector. The Z-1.5mm and Z+1.5mm locations are planes that are 1.5mm lower and 1.5mm higher than the location of the impulse. In figure 1, the total tomographic-angle TA=20^0 and the reconstruction-slice-spacing RSS=1mm. The x axis represents the pixel location in the column containing the impulse, and the y axis is the normalized impulse response's amplitude. In figure 1, (a), (b), and (c) represent three selected candidate algorithms of SAA, MITS, and FBP respectively. We found that there was no substantial difference for 11, 21 and 41 projection numbers with SAA. With a larger N, the MITS preformed much better and clearly reduced more high frequency oscillation, and provided clearer structure. FBP preformed slightly better in out-of-plane structure removal at the larger N due to better sampling in frequency space.

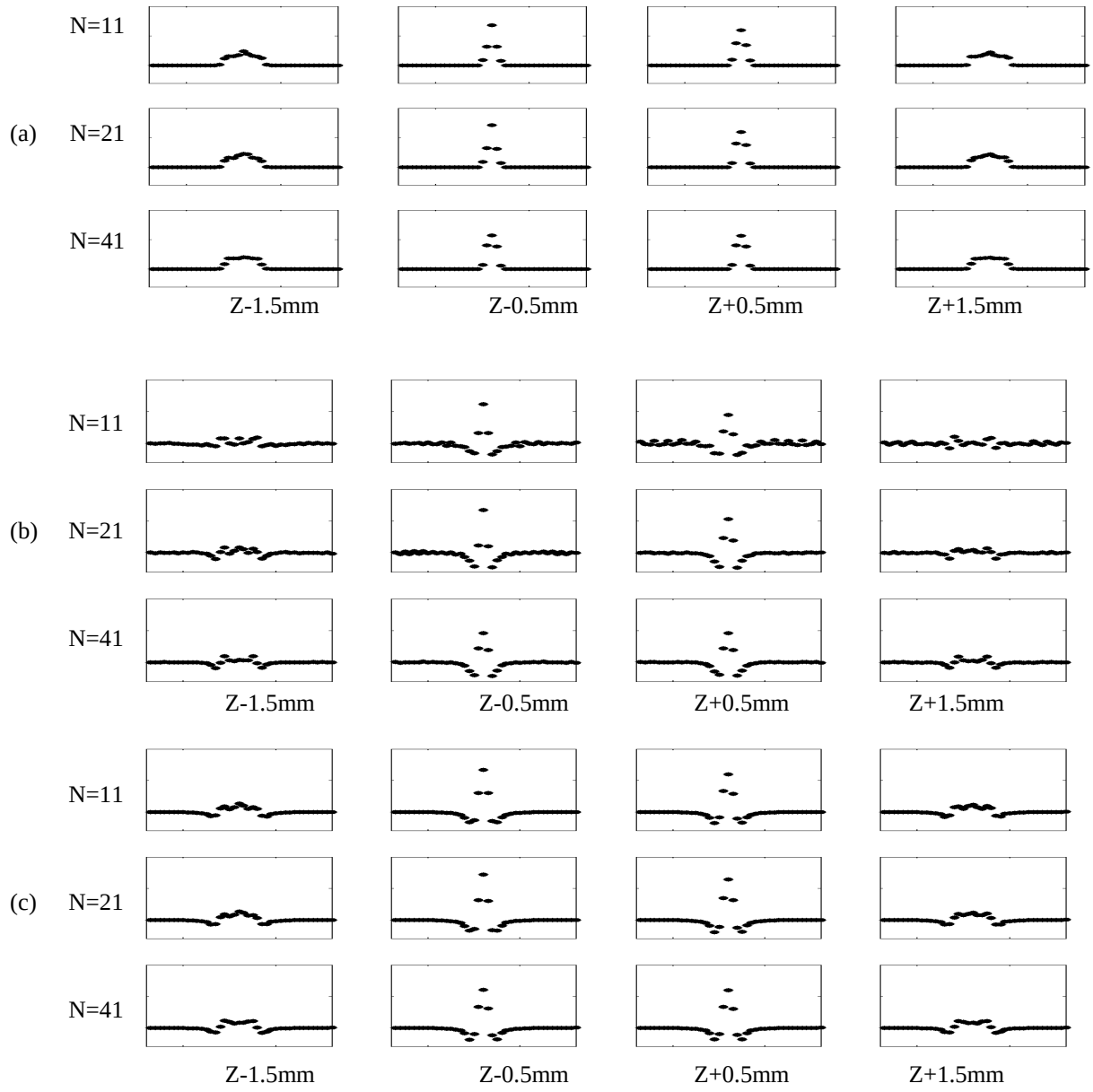

Figure 1. Out-of-plane impulse response, near chest wall: (a) SAA (b) MITS (c) FBP

Work for the specific task 1.2.1 resulted in a proceedings abstract at AAPM, a scientific conference for medical imaging in 2006. In the abstract, we used the impulse response analysis method to demonstrate the improved reconstruction of two-dimensional SAA compared with traditional SAA algorithm (reportable outcome #2).

1.2.2. Analyze the MTF curves of different acquisition parameters for each candidate algorithm. (Months 8-9)

During the investigation, we recognized that the MTF measurement actually includes two parts: 1) the system MTF of the detector; 2) the reconstruction MTF associated with specific reconstruction algorithm and acquisition parameters. The system MTF describes the measured MTF of the detector. A previously published edge method [17,18] was applied at a range of tube angles to see if there is any difference with angle. Figure 2 shows the measured system MTF when X-ray tube is located at different angular locations. The MTF varied little with different angles. The averaged MTF was calculated and served as the system MTF of the detector.

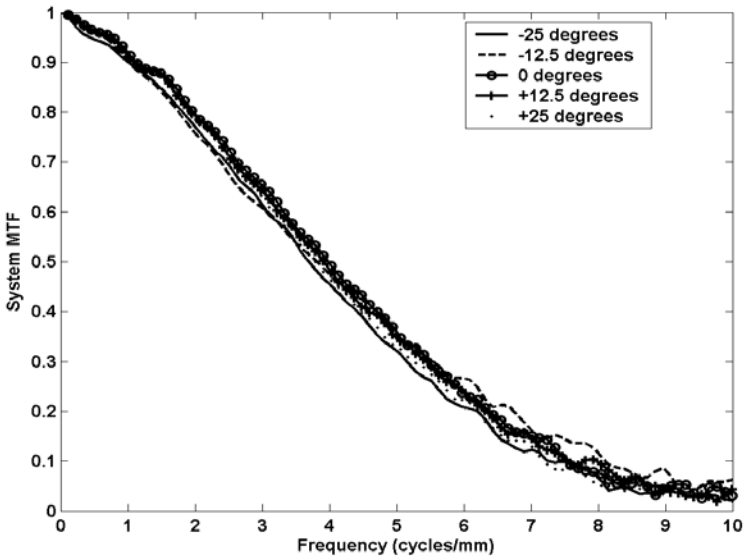

Figure 2. System MTF

The reconstruction MTF was calculated as the Fourier transform of the impulse response on the reconstruction plane associated with specific reconstruction algorithm and acquisition parameters. Figure 3 shows an example how we calculated the reconstruction MTF. A data set of tomosynthesis projection images of a delta function at 40 mm above the detector surface plate and 40 mm away the chest wall was simulated with acquisition parameters of N=25, TA=25^0 and RSS=1 mm. The simulated tomosynthesis sequence was reconstructed by point-by-point back projection (BP) algorithm. Figure 3(a) shows the impulse response where x and *y* axes represents the pixel location on the image. Figure 3(b) represents the reconstruction MTF. Figure 4 shows the total MTF as the combination of the measured system MTF and calculated reconstruction MTF along tube's motion direction and the direction orthogonal to tube's motion.

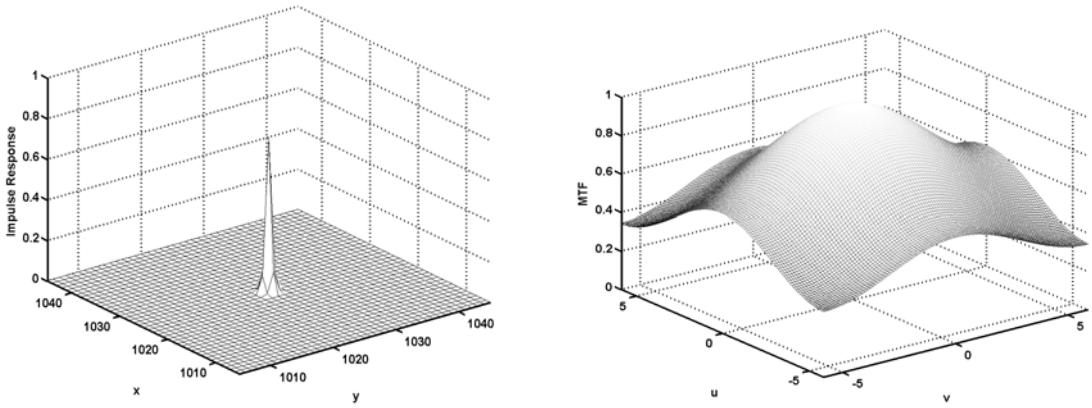

(a) (b)

Figure 3. Point-by-point BP with N=25 and TA=25^0: (a) impulse response; (b) MTF

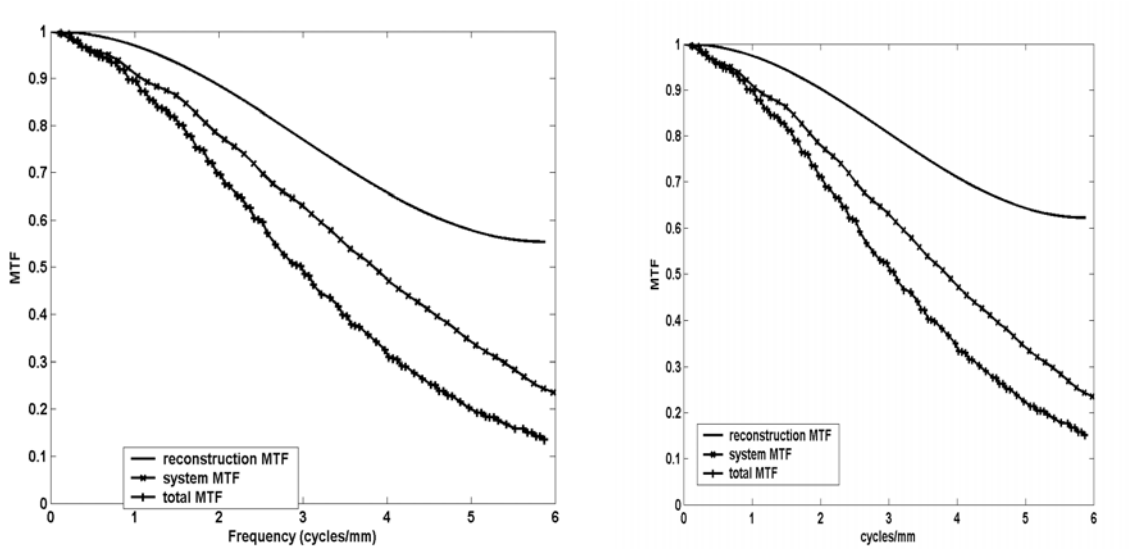

(a) (b)

Figure 4. Reconstruction, system, and total MTFs: (a) direction orthogonal to tube's motion direction (b) tube's motion direction

We applied the impulse response and MTF analysis methods in section 1.2.1 and 1.2.2 to a comparison of BP and SAA algorithms. It resulted in part of a manuscript we submitted to Medical Physics for peer-reviewed journal publication (reportable outcome #1).

1.2.3 Analyze the NPS curves of different acquisition parameters for each candidate algorithm. (Months 10-12)

We did the NPS measurement and analysis of selected candidate algorithms of SAA, MITS and FBP for comparison and optimization. We acquired tomosynthesis sequences of flat images with five different imaging acquisition techniques: 1) N=13, TA=50^0; 2) N=13, TA=25^0; 3) N=25, TA=50^0; 4) N=25, TA=25^0; 5) N=49, TA=50^0. The total exposures were same for tomosynthesis sequences with different acquisition techniques. Three reconstruction-slice-spacings (RSS) of 1mm, 2mm, and 4mm were used for comparison. We also simulated and reconstructed projection

images of a two-dimensional square to match gains and offsets for different candidate reconstruction algorithms and imaging technique parameters. Our previously published methods [19] were applied to calculate the NPS. Figure 5 shows an example of our NPS analysis for MITS algorithm with different acquisition techniques with RSS=1mm.

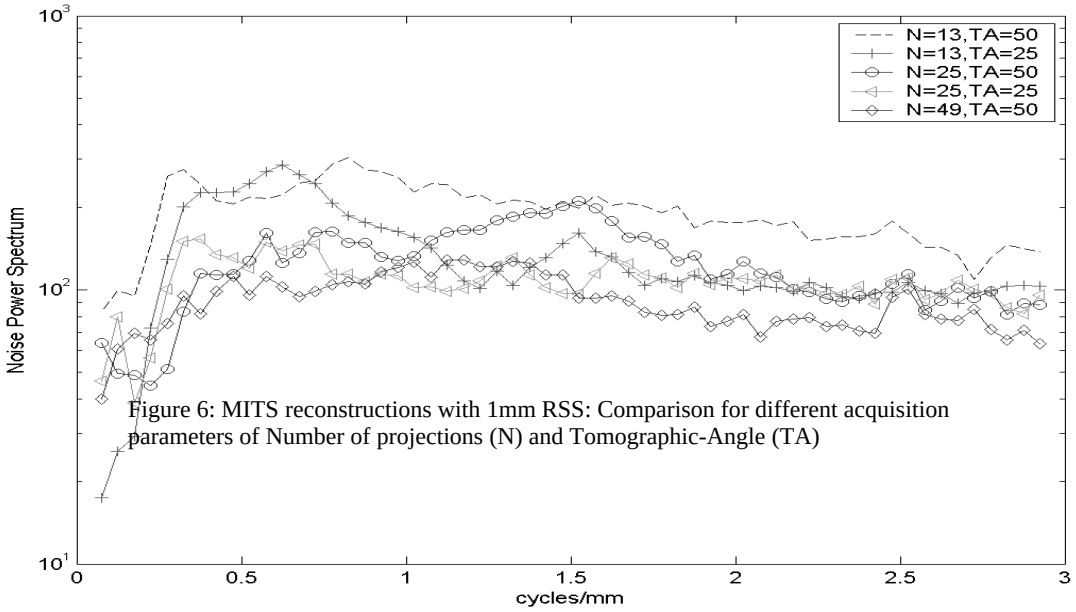

Figure 6: MITS reconstructions with 1mm RSS: Comparison for different acquisition parameters of Number of projections (N) and Tomographic-Angle (TA)

Figure 5: MITS reconstructions with 1mm RSS: Comparison for different acquisition parameters of Number of projections (N) and Tomographic-Angle (TA)

We found that with the same acquisition parameters of *N=49* and *TA=50^0*, the SAA and FBP showed no difference when we varied the *RSS*. The NPS from FBP reconstructions showed reduced NPS at high frequencies due to the applied low-pass Hamming and Gaussian filters. For MITS reconstruction, compared with 2mm and 4mm slice spacing, 1mm slice spacing has better noise response at low-to-middle frequency range. At middle to high frequency range, their noise responses were similar. These are also true for other four acquisition parameters of *N=25* and *TA=50^0*, *N=25* and *TA=25^0*, *N=13* and *TA=50^0*, *N=13* and *TA=25^0*.

Work for the specific task 1.2 resulted in a proceedings paper at SPIE, the primary scientific conference for medical imaging in 2007 (reportable outcome #3). We realized that the NPS itself is not an appropriate method for comparison of different algorithms due to different resolution of each algorithm. In the paper, we proposed a methodology of noise-equivalent quanta NEQ (f) analysis as a better way to compare and optimize different algorithms and acquisition parameters.

Task 2. Comparison of different candidate tomosynthesis reconstruction methods (Months 13-24):

Generally speaking, from impulse response, MTF, and NPS analysis, we found that MITS and FBP performed better with bigger N and wider TA (such as N=49 and TA=50^0). MITS

performed better with smaller RSS (RSS=1mm). We also found from experiments that N=25, TA=50^0, RSS=1mm is an efficient way in clinical application for MITS and FBP. We have proposed a methodology of NEQ (f) analysis to compare and optimize reconstruction algorithms and acquisition techniques. We are working on the NEQ (f) analysis now and expect to finish the NEQ (f) analysis in May 2007. Once technique parameters have been optimized, we will conduct the comparison of different candidate tomosynthesis reconstruction methods based on the lesion simulation and human observer study.

KEY RESEARCH ACCOMPLISHMENTS

- Investigated several different reconstruction algorithms for digital breast tomosynthesis, including SAA, NIKL, BP, MITS, FBP, MLEM. Selected candidate algorithms and compared performance against each candidate algorithms.
- Analyzed impulse response, MTF, and NPS by simulation, experiments and characterization to compare and optimize the imaging acquisition parameters including total Tomographic-Angle (TA), Number of projection images (N), and Reconstruction-Slice-Spacing (RSS).
- Investigated the importance of point-by-point BP for isocentric motion in digital breast tomosynthesis, especially for reconstruction of small structures such as microcalcifications. Proposed a methodology of NEQ (f) analysis for comparison and optimization.

REPORTABLE OUTCOMES

The following manuscripts and abstract are attached at appendices 1, 2 and 3 with the same numbers. The names of the fellow (Chen) and mentor (Dobbins) are boldfaced for emphasis.

1. **Y. Chen**, J. Y. Lo, and **J. T. Dobbins III.**, "Importance of point-by-point Back Projection (BP) correction for isocentric motion in digital breast tomosynthesis: relevance to morphology of microcalcifications," *Med. Phys, in review, 2007.*
2. **Y. Chen**, J. Y. Lo, **J. T. Dobbins III**, "Two-dimensional Shift-And-Add Algorithm for Digital Breast Tomosynthesis Reconstruction," *Med. Phys. 33 (6), 2001 (2006).*
3. **Y. Chen**, J. Y. Lo, N. T. Ranger, E. Samei, **J. T. Dobbins III**, "Methodology of NEQ(f) analysis for optimization and comparison of digital breast tomosynthesis acquisition techniques and reconstruction algorithms," *Proc. SPIE 6510, 65101-I, (2007).*

CONCLUSIONS

We have investigated different reconstruction algorithms for digital breast tomosynthesis, compared and optimized candidate algorithms. We have analyzed the impulse response, MTF, and NPS by simulation, experiments, and computation to compare and optimize candidate algorithms and different acquisition parameters. We also proposed a NEQ(f) analysis to better compare and optimize reconstruction algorithms and acquisition techniques. Future work will be done to further compare the algorithms with optimized acquisition parameters by lesion simulation and human observer study.

REFERENCE

1. Ralph Highnam, Michael Brady, "Mammographic Image Analysis", Kluwer Achademic Publishers, Dordrecht, The Netherlands, 1999.

2. Lawrence W. Bassett, Valerie P. Jackson, Karin L. Fu, Yao S. Fu, "Diagnosis of Diseases of the Breast", 2nd ed, Elsevier Saunders, Philadelphia, Pennsylvania, 2005.
3. Loren T. Niklason, et al., "Digital tomosynthesis in breast imaging", Radiology 205: 399-406, 1997.
4. Tao Wu, et al., "Tomographic mammography using a limited number of low-dose cone-beam projection images", Med. Phys. 30 (3): 365-380, March 2003.
5. Tao Wu, R. H. Moore, E. A. Rafferty, D. B. Kopans, "A comparison of reconstruction algorithms for breast tomosynthesis", Med. Phys. 9: 2636-2647, September 2004.
6. S. Suryanarayanan, A. Karellas, S. Vedantham, S. J. Glick, C. J. D'Orsi, S. P. Baker, and R. L. Webber, "Comparison of tomosynthesis methods used with digital mammography," Acad. Radiol. **7**, 1085-1097 (2000).
7. S. Suryanarayanan, A. Karellas, S. Vedantham, S. P. Baker, S. J. Glick, C. J. D'Orsi, S. P. Baker, and R. L. Webber, "Evaluation of linear and nonlinear tomosynthetic reconstruction methods in digital mammography," Acad. Radiol. **8**, 219-224 (2001).
8. L. Zhou, J. Oldan, P. Fisher, and G. Gindi, "Low-contrast lesion detection in tomosynthetic breast imaging using a realistic breast phantom," Proc. SPIE **6142**, 1685-1696 (2006).
9. Y. Zhang, H. Chan, B. Sahiner, J. Wei, M. M. Goodsitt, L. M. Hadjiiski, J. Ge, C. zhou, "A comparative study of limited-angle cone-beam reconstruction methods for breast tomosynthesis," Med. Phys. 33(10), 3781-3795 (2006).
10. J. T. Rakowski and M. J. Dennis, "A comparison of reconstruction algorithms for C-arm mammography tomosynthesis," Med. Phys. 33(8), 3018-3032 (2006).
11. Tao Wu, R. H. Moore, E. A. Rafferty, D. B. Kopans, "A comparison of reconstruction algorithms for breast tomosynthesis," Med. Phys. **9**, 2636-2647 (2004).
12. Y. Chen, J. Y. Lo, J. A. Baker, J. T. Dobbins III, "Gaussian frequency blending algorithm with Matrix Inversion Tomosynthesis (MITS) and Filtered Back Projection (FBP) for better digital breast tomosynthesis reconstruction," Proc. SPIE **6142**, 122-130 (2006).
13. T. Mertelemeier, J. Orman, W. Haerer, and M. K. Dudam, "Optimizing filtered backprojection reconstruction for a breast tomosynthesis prototype device," Proc. SPIE **6142**, 131-142 (2006).
14. Y. Chen, J. Lo, J. T. Dobbins III, "Matrix Inversion Tomosynthesis (MITS) of the Breast: Preliminary Results," in *RSNA 90th Scientific Assembly*, Chicago, IL, 2004.
15. J. T. Dobbins, III., "Matrix Inversion Tomosynthesis improvements in longitudinal x-ray slice imaging", U.S. Patent #4,903,204 (1990). Assignee: Duke University.
16. Y. Chen, J. Y. Lo, J. T. Dobbins III, "Impulse response analysis for several digital tomosynthesis mammography reconstruction algorithms," Proc. SPIE **5745**, 541-549 (2005).
17. R. S. Saunders, E. Samei, J. Jesneck, J. Lo, "Physical characterization of a prototupe selenium-based full field digital mammography detector," *Med. Phys. 32(2), 588-599 (2005).*
18. R. S. Saunders and E. Samei, "A method for modifying the image quality parameters of digital radiographic images," *Med. Phys. 30, 3006-3017 (2003).*
19. J. T. Dobbins III, D.L. Ergun, L. Rutz, D. A. Hinshaw, H. Blume, D. c. Clark, "DQE (f) of four generations of comouted radiography acquisition devices", *Med. Phys. 22 (10): 1581-1593 (1995).*

Importance of point-by-point Back Projection (BP) correction for isocentric motion in digital breast tomosynthesis: relevance to morphology of structures such as microcalcifications

Ying Chen
Department of Biomedical Engineering
Duke Advanced Imaging Laboratories
Duke University, Durham, NC 27710

Joseph Y. Lo
Departments of Radiology and Biomedical Engineering
Duke Advanced Imaging Laboratories
Medical Physics Graduate Program
Duke University, Durham, NC 27710

James T. Dobbins, III
Departments of Radiology and Biomedical Engineering
Duke Advanced Imaging Laboratories
Medical Physics Graduate Program
Duke University, Durham, NC 27710

A manuscript for publication in *Medical Physics*

PLEASE DO NOT COPY OR DISTRIBUTE

ABSTRACT

Digital breast tomosynthesis is a three-dimensional imaging technique that provides an arbitrary set of reconstruction planes in the breast from a limited-angle series of projection images acquired while the x-ray tube moves. Traditional Shift-And-Add (SAA) tomosynthesis reconstruction is a common mathematical method to line up each projection image based on its shifting amount to generate reconstruction slices. With parallel-path geometry of tube motion, the path of the tube lies in a plane parallel to the plane of the detector. The traditional SAA algorithm gives shift amounts for each projection image calculated only along the direction of x-ray tube movement. However, with the partial isocentric motion of the x-ray tube in breast tomosynthesis, small objects such as microcalcifications appear slightly blurred (for instance, about 1~10 pixels in blur for a microcalcification in a human breast) in traditional SAA images in the direction perpendicular to the direction of tube motion. Furthermore, out-of-plane objects manifest themselves as arc-shaped blurs due to the isocentric motion. Some digital breast tomosynthesis algorithms reported in the literature utilize a traditional one-dimensional SAA method that is not wholly suitable for isocentric motion. In this paper, a point-by-point back projection (BP) method is described and compared with traditional SAA for the important clinical task of evaluating morphology of small objects such as microcalcifications. Impulse responses at different 3-D locations with five different combinations of imaging acquisition parameters were investigated. Reconstruction images of microcalcifications in a human subject were also evaluated. Results showed that with traditional SAA and 50^0 angular range of tube movement, the in-plane blur and arc-shaped out-of-plane artifacts were obvious for objects farther away from x-ray source. In a human subject, the appearance of calcifications was blurred in the direction

orthogonal to the tube motion and the out-of-plane artifact of calcifications was curvilinear with traditional SAA. With point-by-point BP, the appearance of calcifications was sharper. The point-by-point BP method demonstrated improved rendition of microcalcifications in the direction perpendicular to the tube motion direction. With wide angles or for imaging of larger breasts, this point-by-point BP rather than the traditional SAA should also be considered as the basis of further deblurring algorithms that work in conjunction with the BP method.

KEYWORDS

mammography, tomosynthesis, 3D reconstruction, Shift-And-Add (SAA), Back Projection (BP), microcalcifications

1. INTRODUCTION

Breast cancer is the most common cancer among women. Currently, mammography is the most important and efficacious tool for the early detection of breast cancer.[1] However, limitations of mammography have been well publicized, such as 20% false negative rate [2,3], many callbacks from screening, and low positive predictive value of about 15-34% from biopsy.[4,5] It can be difficult for conventional two-dimensional mammography to distinguish a cancer from overlying breast tissues.

Digital breast tomosynthesis is a three-dimensional imaging technique that provides an arbitrary set of reconstruction planes in the breast from a limited-angle series of projection images when the x-ray tube moves [6]. There are a variety of tomosynthesis reconstruction algorithms, including the image-stretching method proposed by Niklason and colleagues[7], Maximum Likelihood iterative algorithm by Wu *et al*. [8], tuned-aperture computed tomography (TACT) reconstruction methods developed by Webber and investigated by Suryanarayanan *et al*[10, 11], algebraic reconstruction techniques (ART) [29, 31, 32], filtered back projection (FBP) [9, 14, 20], and matrix inversion tomosynthesis (MITS) [13]. Some of these algorithms depend on a traditional Shift-And-Add (SAA) method that is appropriate for parallel-path geometries. For example, Niklason and colleagues modified the traditional shift-and-add technique for mammography to stretch the image along the direction of x-ray tube motion to account for the effects of magnification variation with angle, but the correction necessary along the direction perpendicular to the tube motion was not taken into account[7]. Suryanarayanan *et al* applied Webber's TACT method to breast tomosynthesis reconstruction [10, 11], and used traditional SAA. The MITS technique

developed in our laboratory has been investigated for breast tomosynthesis using a traditional SAA algorithm as the basis for subsequent matrix inversion deblurring.[13]

Traditional SAA is appropriate for parallel-path tube movement when the path of the tube lies in a plane parallel to the plane of the detector [6]. However, the partial isocentric motion of the tube in breast tomosynthesis causes a non-parallel motion. While the effects due to isocentric motion are small for most objects, the use of SAA methods introduces morphological distortions with small objects such as microcalcifications. Therefore, a simple SAA reconstruction algorithm is not entirely suitable for breast tomosynthesis. This issue of non-parallel motion is addressed in point-by-point Back Projection (BP) methodologies [9], but its impact has largely not been evaluated with algorithms that rely on simply traditional SAA approaches. This paper demonstrates the importance of point-by-point corrections for isocentric motion in digital breast tomosynthesis by examining how the morphology of microcalcification reconstructions changes relative to a traditional SAA method that does not employ point-by-point corrections.

In this paper, a point-by-point BP correction method is described and compared with traditional SAA by analysis of impulse response. Impulse responses at different 3-D locations with five different combinations of imaging acquisition parameters were investigated. In addition, reconstructed images of a calcification in a human subject were evaluated to demonstrate the improvement in the morphology of microcalcifications associated with the point-by-point BP correction method.

2. METHODS

A. Breast tomosynthesis system

A selenium-based direct conversion Siemens Mammomat Novation DR prototype system was modified to be used as the breast tomosynthesis acquisition system.[21] The detector area was 24cm× 30cm (2816 × 3584 pixels), with a pixel pitch of 85 μm (different from that used in the clinical digital mammography system from the same manufacturer). The exposure and readout cycle was 0.8 sec per image. Several different modes were provided to choose from different available projection numbers, total angular range and speeds. Figure 1 shows a diagram of the breast tomosynthesis imaging system. During the tomosynthesis procedure, the x-ray tube moves automatically along an arc above the chest wall to acquire up to 49 projection images with a total angular range of $0\text{-}50^0$ at the rotation center. A continuous x-ray motion was employed. The rotation center to detector distance *R* is 6 cm. A compression paddle is used to keep the object still.

B. Traditional Shift-And-Add (SAA) algorithm

The traditional Shift-And-Add (SAA) tomosynthesis reconstruction algorithm [6,12] is a common mathematical method to line up each projection image based on its relative shift to generate reconstruction slices at specified depths. When the x-ray tube moves, objects at different heights above the detector will be projected onto the detector at positions depending on the relative heights of the objects.

In order to reconstruct slice images of the breast, each projection image should be shifted by an amount appropriate for the plane of reconstruction. If the detector remains stationary and the tube moves in a plane that is parallel to the detector plane, the

magnification of objects depends only on the height of the object. With the traditional Shift-And-Add (SAA) algorithm for breast tomosynthesis reconstruction, shift amounts for each projection plane are calculated one dimensionally along the axis of x-ray tube movement. In this paper, the shift amount was calculated based on projected positions from central points of each reconstruction plane. The shifted planes were added together to emphasize structures in the in-focus plane and blur out structures in other planes.

As shown in figure 1, plane *S* represents a reconstruction plane at a height of *Z* above the detector surface. When the x-ray tube moves, objects in plane *S* will be projected onto the detector surface. For a specific projection image from angle θ, in order to shift the projection image to line up structures from plane *S*, the one-dimensional SAA algorithm uses the shift amount calculated as:

$$shift_i(Z) = P_i(Z) = L \cdot \sin\theta \cdot \frac{Z}{L \cdot \cos\theta + (R - Z)} \tag{1}$$

where *L* is length of the rotation arm, and *R* is the height of the rotation axis from the detector surface. One can obtain the reconstruction plane *S* as the average of all *N* shifted projection images:

$$T(x, y) = \frac{1}{N} \sum_{i=1}^{N} I_i(x, y) \otimes \delta[y - shift_i(Z)] \tag{2}$$

C. Point-by-point Back Projection (BP) algorithm

Because of the isocentric motion of the x-ray tube, a shift actually occurs in both x and y directions on each projection image. Figure 2 shows the arc path of motion when the x-ray tube moves along the *y* axis. Point *A* represents a single structure on a certain reconstruction plane. P_i, P_j, P_k are the actual projected locations of point *A* on the detector

with different x-ray tube locations of T_i, T_j, T_k. The actual path of projected locations follows a two-dimensional arc rather than a one-dimensional line. Therefore, to reconstruct a single pixel on a reconstruction plane at certain height about the detector, the shift amount should be considered along both x and y directions.

With the point-by-point BP algorithm, shift amounts for every pixel location on each reconstructed plane were computed, taking into account the 2D arc projection location of reconstructed objects in each plane. In figure 2, (Ax, Ay, Az) represent coordinates of point A. (Tx_i, Ty_i, Tz_i) represents the tube position along the x, y, z axes when the tube moves to position T_i. (Px_i, Py_i, Pz_i) represents projected coordinates of point A on the projection image. One can calculate the two-dimensional shift amount as:

$$\begin{aligned} Px_i &= Tx_i - \frac{(Tx_i - Ax)(Tz_i - Pz_i)}{Tz_i - Az} \\ Py_i &= Ty_i - \frac{(Ty_i - Ay)(Tz_i - Pz_i)}{Tz_i - Az} \end{aligned} \tag{3}$$

Since P_i is located on the detector, one can define $Pz_i = 0$. Thus, the above formula can be simplified as:

$$\begin{aligned} Px_i &= Tx_i + \frac{(Tx_i - Ax)Tz_i}{Tz_i - Az} \\ Py_i &= Ty_i + \frac{(Ty_i - Ay)Tz_i}{Tz_i - Az} \end{aligned} \tag{4}$$

The final pixel value of point A in the tomosynthesized reconstruction was calculated as: $\frac{1}{N}\sum_{i=1}^{N} I(P_i)$, where $I(P_i)$ is the pixel value at a given location on the i^{th} projection image, and N is the total number of projection images. In this paper, bilinear interpolation was used to address the issue of partial pixel locations. Computation times for the point-

by-point BP algorithm are roughly comparable to the SAA method. With a computer of 800 MHz CPU and UNIX operating system, it takes less than 5 minutes for either the point-by-point BP or traditional SAA reconstruction.

D. Impulse response analysis

A single delta function was simulated by ray-tracing method as the input impulse to investigate the sharpness of reconstructed in-plane structures and to see how the traditional SAA and point-by-point BP algorithm differ from each other. Two different impulse locations were investigated in this paper: 1) an impulse that is exactly underneath the x-ray source (near the chest wall) and in a defined reconstructed plane (40mm above the detector surface); 2) an impulse that is approximately 4 cm away from the chest wall and in a defined reconstructed plane (40mm above the detector surface). Parameters of the digital breast tomosynthesis device described in section 2A were used for geometries of the simulation. Five different combinations of acquisition parameters including projection image numbers and total angular range were applied: 1) 13 projections with 25^0 angular range; 2) 13 projections with 50^0 angular range; 3) 25 projections with 25^0 angular range; 4) 25 projections with 50^0 angular range; and 5) 49 projections with 50^0 angular range. For each impulse location and combination of acquisition parameters, two datasets of projection images were simulated by ray-tracing method: 1) background-only: only $1/r^2$ shading difference for each pixel on projection images was taken into account (r is the distance from the x-ray source to each pixel location); 2) impulse-added: projection images with simulated impulse and the $1/r^2$ shading difference. Other system blur and noise issues were not addressed in this paper to focus on the contribution of the blur due to the isocentric motion. During ray-tracing, if the simulated impulse was projected onto

non-integer pixel location on the detector surface, linear interpolation of the projected impulse among four neighboring pixels was performed.

Traditional SAA and point-by-point BP reconstruction algorithms were applied to both impulse-added and background-only simulated tomosynthesis projection sequences. A reconstruction plane spacing of 1 mm was used. Reconstruction images from background-only projections were subtracted from reconstructions of impulse-added projections to eliminate background shading effects. The impulse responses were normalized based on the ideal condition when the impulse is exactly located underneath the x-ray source.

E. Human subject images

Human subject images have been acquired on our prototype breast tomosynthesis system under an IRB-approved protocol. Images of one human subject with notable calcifications were reconstructed with the traditional SAA and point-by-point BP methods to demonstrate the effect of the point-by-point BP method on reconstructed calcification morphological appearance. A tomosynthesis sequence was acquired with twenty-five projection images and a total angular range of 50^0. The radiographic technique for breast tomosynthesis was selected using technique optimization procedures reported previously [33]. The target/filter for tomosynthesis exams is always W/Rh. The kVp is selected to maximize a figure of merit (signal difference to noise ratio squared per unit dose) for a given breast thickness and density. Then the mAs can be chosen to maintain image quality while reducing dose when compared against the conventional Mo/Mo or Mo/Rh technique, or alternatively to improve quality while maintaining dose.

For this specific subject, we chose to do the latter. By using the tomosynthesis technique of W/Rh at 28 kVp (HVL 0.50 mm Al) and 112 mAs for this 100% fatty, 33 mm breast, we maintained the same dose as the conventional left cranio caudal (LCC) mammogram.

3. RESULTS

A. Impulse responses

Figures 3, 4, and 5 show the impulse response results with a simulated impulse located in a defined reconstruction plane at 40 mm above the detector, and approximately 4 cm away from the chest wall. Figure 3 shows results from simulated acquisition parameters of 25 projections and 50^0 total tube angular movement. Figure 4 shows results from 13 projections and 50^0 angular movement. Figures 5 shows results from 25 projections and a narrower angular range of 25^0. On figures 3 through 5, (a) and (c) give corresponding values in a plane at the exact height of the impulse's location; (b) and (d) give the impulse response of reconstruction planes 1 mm lower than the impulse's location; (a) and (b) are results from point-by-point BP, (c) and (d) are results from traditional SAA. The *x* and *y* axes give the pixel location on the reconstruction plane, and the plot displays the normalized amplitude of the response. X axis represents the direction orthogonal to tube's motion direction. Y axis represents the tube's motion direction. Only a 40×40 pixel region close to the impulse is shown for clarity.

One can see that with traditional SAA, when the impulse is 4 cm away from the chest wall and the x-ray source moves along a wider angular range of 50^0, the in-plane response is noticeably blurred and multiple peaks exist in a direction that is perpendicular to the direction of tube movement (Fig. 3c and 4c), reflecting the uncorrected partial isocentric tube motion. With point-by-point BP, the in-plane response is much sharper (Fig. 3a and 4a), and the out-of-plane blur responses are less curved compared with that of traditional SAA (Fig. 3b, 2d and 4b, 4d). When the number of projection images decreases to 13, the in-plane response and out-of-plane blur become discrete (Fig. 4b, 4d)

due to limited projection numbers. With a narrower angular range of 25^0, the differences between traditional SAA and point-by-point BP are less obvious (Fig. 5). However, one can still say that the in-plane response of point-by-point BP is higher and sharper than that of traditional SAA.

Table 1 gives the full width at a half maximum (FWHM) measurement and full width at a tenth maximum values (FWTM) of the in-plane impulse responses along two orthogonal directions when the impulse is located at 40 mm above the detector surface and near chest wall. Table 2 gives the same measurements of FWHM and FWTM when the impulse is located 4 cm away chest wall. When the impulse is located near the chest wall (underneath the x-ray tube), there is only a small difference (< 1 pixel size) in FWHM and FWTM values between traditional SAA and point-by-point BP for each combination of acquisition parameters. With a narrower angle of 25^0, differences are small too (less than 1 pixel size). However, with a wider tube angular movement range of 50^0, when the impulse is located 4 cm away the chest wall, major differences exist along the *X* axis (direction orthogonal to tube's motion direction). Multiple peaks and blurs appear along this direction (Fig. 3c and 4c). Due to multiple peaks along the *X* axis, FWHM cannot adequately represent the real extension of impulse response; for that reason, the measurement of FWTM was also provided. The difference in FWTM values is as large as 9 pixels between traditional SAA and point-by-point BP.

B. Human subject images

Figures 6 shows regions of interest containing two calcifications from images of the left (L) breast of the human subject. Reconstructed structures by traditional SAA and point-

by-point BP methods are compared. A 12.75×12.75 mm region-of-interest (ROI) is demonstrated. Compared with traditional SAA, edges of calcifications are sharper and better focused with point-by-point BP (Fig. 6b and 6e). With traditional SAA, out-of-plane structures appeared curvilinear and indistinct (Fig. 6a and 6c). With point-by-point BP, the in-plane structures are sharper, and the out-of-plane structures appear linear and curvilinear (Fig. 6d and 6f). A quantitative measurement of the shape and width of the punctate calcification (left-most calcification) on this ROI is given in table 3. *Y* axis corresponds to the direction of x-ray tube motion, and *X* axis is the direction orthogonal to the tube motion direction. One can see that, compared with the traditional SAA, point-by-point BP provided clearer edge shape and narrower width along *X* axis that is perpendicular to the x-ray tube motion direction.

Figure 7a is a low dose middle projection image of the same human breast when the x-ray tube was positioned at the 0^0 position. Figures 7b and 7c are reconstructed slice images by traditional one-dimensional SAA and point-by-point BP respectively, at a height of 7.5 mm above the detector. One can find that the rendition of a solitary calcification (when out of the reconstructed plane) appears more curvilinear in the SAA image compared with that in the point-by-point BP image. Also, the reconstructed size of the breast by traditional one-dimensional SAA is larger than that from point-by-point BP (Fig. 7b, 7c). This is due to the uncorrected magnification difference with traditional SAA for structures at different locations in the reconstruction plane. When the structures are located at difference heights above the detector surface, differences in magnification exist. Structures at higher locations above the detector surface will be projected onto the detector with a larger size. Traditional SAA doesn't take this magnification difference

into account. After shift-and-add, structures at higher locations appear larger compared with the same size structure at lower location. The reconstructed structure size from traditional SAA reconstruction cannot reflect the real structure size. Point-by-point BP correctly addressed this magnification difference issue by calculating shift amounts for every pixel location on each reconstruction plane. Therefore, the point-by-point BP reconstructed plane in figure 7c reflects the real size and is smaller than that from traditional SAA.

4. DISCUSSION

With the traditional SAA algorithm for digital breast tomosynthesis reconstruction, shift amounts for each projection plane are calculated only along the axis of the x-ray tube's movement. However, due to the isocentric motion of x-ray tube, the track of projected impulse locations actually occurs in two dimensions on the detector. As a result, the in-plane structures are blurred and the out-of-plane structures have curve-shaped appearance. Illustrations with impulse responses and reconstructed human subject images demonstrated that this is an inherent problem of traditional one-dimensional SAA with breast tomosynthesis. This problem is more obvious when the object is farther away from the chest wall and higher above the detector. Thus, with traditional SAA, objects such as microcalcifications appear slightly blurred in the direction perpendicular to the direction of tube motion, and their apparent morphology changes.

With point-by-point BP, the artifacts coming from the isocentric x-ray tube's movement are corrected. The in-plane structures are sharper. While reconstructions of gross anatomy were adequate with either algorithm, the morphology of small structures such as microcalcifications reconstruction requires a point-by-point correction. Morphological artifacts were reduced with the point-by-point correction, and rendition of small objects such as microcalcifications were greatly improved. These results demonstrate the importance of using a point-by-point correction to remove isocentric motion artifacts in tomosynthesis imaging of the breast, where the morphology of microcalcifications has an important bearing on clinical decision making.

The source of the difficulties with traditional SAA is the variable magnification introduced by the partial isocentric motion of the x-ray tube. The magnification of objects in different reconstruction slices varies from plane-to-plane as a function of the height of slices above the detector. Even within the same reconstruction plane, the magnification also changes at different pixel locations due to the partial isocentric motion. Traditional SAA does not take this issue into account. With point-by-point BP, the shift amount is calculated according to the exact location of the pixel in the reconstruction slices, thereby addressing this issue of variable magnification.

None of methods commonly used for breast tomosynthesis is truly spatially invariant due to the partial isocentric tube motion, although for structures close to the chest wall and near the detector, the imaging system is approximately spatially invariant. Therefore, linear deblurring techniques will demonstrate less uniform behavior in breast tomosynthesis geometries than in parallel-path tomosynthesis geometries. We found that when the impulse is located near the chest wall or when the total angular range is narrower such as 25^0, there is no big difference (<1 pixel size) in FWHM and FWTM values between traditional SAA and point-by-point BP for a reconstruction with a height of 40 mm above the detector. However, with a wider angle of 50^0, even moving the impulse 4 cm away chest wall shows a difference (about 9 pixels) along the direction orthogonal to the direction of tube motion. Therefore, with a narrow angle, or for small or thin breasts, the SAA algorithm may be tolerated. However, with a wide angle or large breast size, the point-by-point BP algorithm rather than traditional SAA should be used to minimize issues related to isocentric motion.

Deblurring algorithms such as FBP or MITS, which are an important component of high-quality tomosynthesis reconstruction, should use the point-by-point BP method rather than the SAA method to generate the constituent images prior to deblurring under the same conditions of wide tube angle or large breast size.

5. CONCLUSIONS

This work demonstrates that point-by-point BP is an effective method to reconstruct 3D tomosynthesis images of the breast with improved rendition of small structures such as microcalcifications. Compared with the traditional SAA algorithm, the method of point-by-point BP takes into account the variable magnification and shift occurring along the direction orthogonal to tube movement due to the isocentric tube motion. Point-by-point BP improves the sharpness and morphology of structures especially for small objects such as calcifications. This may prove helpful to radiologists in discriminating malignant from benign microcalcification patterns, and thereby improve the accuracy of breast cancer detection.

Acknowledgments

We thank Jay A. Baker, M.D., at Duke University Medical Center for clinical insight and helpful discussion. This work was supported by a grant from US Army Breast Cancer Research Program (USAMRMC W81XWH-06-1-0462), a research grant from Siemens Medical Solutions, and NIH/NCI R01 112437.

Figure captions

FIGURE 1. Breast Tomosynthesis Imaging System (***O*** is the rotation center. ***R*** is the rotation center to detector distance. ***L*** is the rotation arm length. ***Z*** is the height of plane ***S*** above the detector.)

FIGURE 2. Two-dimensional arc path from isocentric tube motion

FIGURE 3. Traditional SAA and point-by-point BP impulse responses: 25 projection images and 50^0 angular range, with the impulse located 40mm above the detector and about 4cm away from the chest wall. (a) and (b) give the impulse response of point-by-point BP; (c) and (d) give the impulse response of traditional SAA. (a) and (c) are impulse responses in the plane at the exact height of the impulse's location; (b) and (d) give corresponding values in a reconstruction plane 1 mm below the impulse's location.

FIGURE 4. Traditional SAA and point-by-point BP impulse responses: 13 projection images and 50^0 angular range, with the impulse located 40mm above the detector and about 4cm away from the chest wall. (a) and (b) give the impulse response of point-by-point BP; (c) and (d) give the impulse response of traditional SAA. (a) and (c) are impulse responses in the plane at the exact height of the impulse's location; (b) and (d) give corresponding values in a reconstruction plane 1 mm below the impulse's location.

FIGURE 5. Traditional SAA and point-by-point BP impulse responses: 25 projection images and 25^0 angular range, with the impulse located 40mm above the detector and about 4cm away from the chest wall. (a) and (b) give the impulse response of point-by-

point BP; (c) and (d) give the impulse response of traditional SAA. (a) and (c) are impulse responses in the plane at the exact height of the impulse's location; (b) and (d) give corresponding values in a reconstruction plane 1 mm below the impulse's location.

TABLE 1. The impulse is located near chest wall. Full width at half maximum (FWHM) and full width at tenth maximum (FWTM) measurements of in-plane impulse response along two directions: tube's motion direction (Y axis) and direction orthogonal to tube's motion (X axis).

Table 2. The impulse is located 4 cm away chest wall. Full width at half maximum (FWHM) and full width at tenth maximum (FWTM) measurements of in-plane impulse response along two directions: tube's motion direction (Y axis) and direction orthogonal to tube's motion (X axis).

FIGURE 6. Reconstructed 12.75×12.75mm ROI of a human breast containing calcifications, Z=18 mm represents the plane height closet to the location of the calcification: (a) Traditional SAA, Z=16.5mm; (b) Traditional SAA, Z=18mm; (c) Traditional SAA, Z=19.5mm; (d) Point-by-point BP, Z=16.5mm; (e) Point-by-point BP, Z=18mm; (f) Point-by-point BP, Z=19.5mm

TABLE 3. Quantitative measurement of the leftmost calcification depicted in Fig. 6.

FIGURE 7. A human breast demonstrating a solitary calcification: (a) Low dose middle (0^0) projection image of the tomosynthesis sequence. The spectrum used for the tomosynthesis sequence was 28 kVp with W/Rh targer/filter and 112.5 mAs for a total of

25 projection images and 50^0 angular range. (b) Traditional SAA reconstructed slice

440 image: Z=7.5mm. (c) Point-by-point BP reconstructed slice image: Z=7.5mm

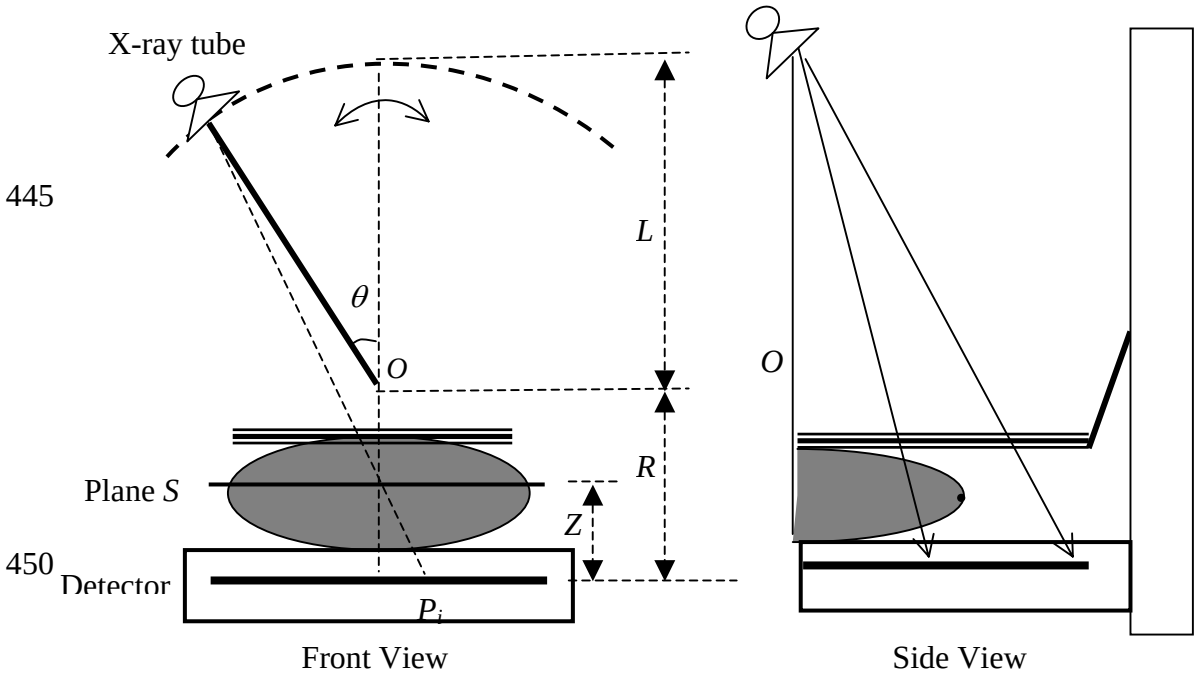

FIG. 1. Breast Tomosynthesis Imaging System (***O*** is the rotation center. ***R*** is the rotation center to detector distance. ***L*** is the rotation arm length. ***Z*** is the height of plane ***S*** above the detector.)

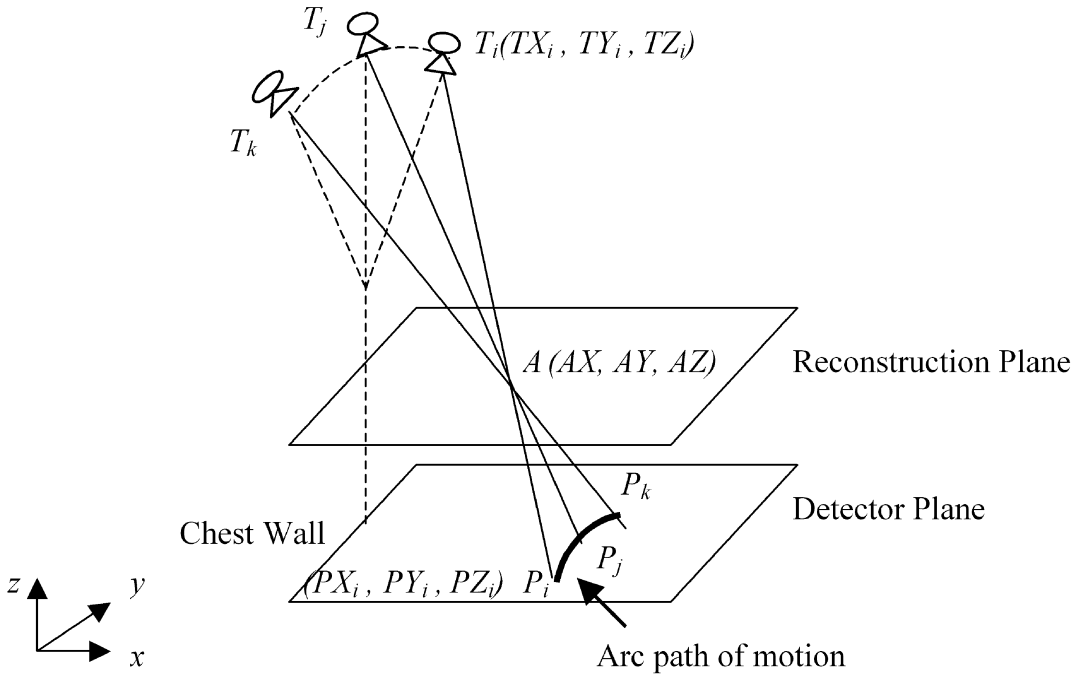

FIG. 2. Two-dimensional arc path from isocentric tube motion

460

460

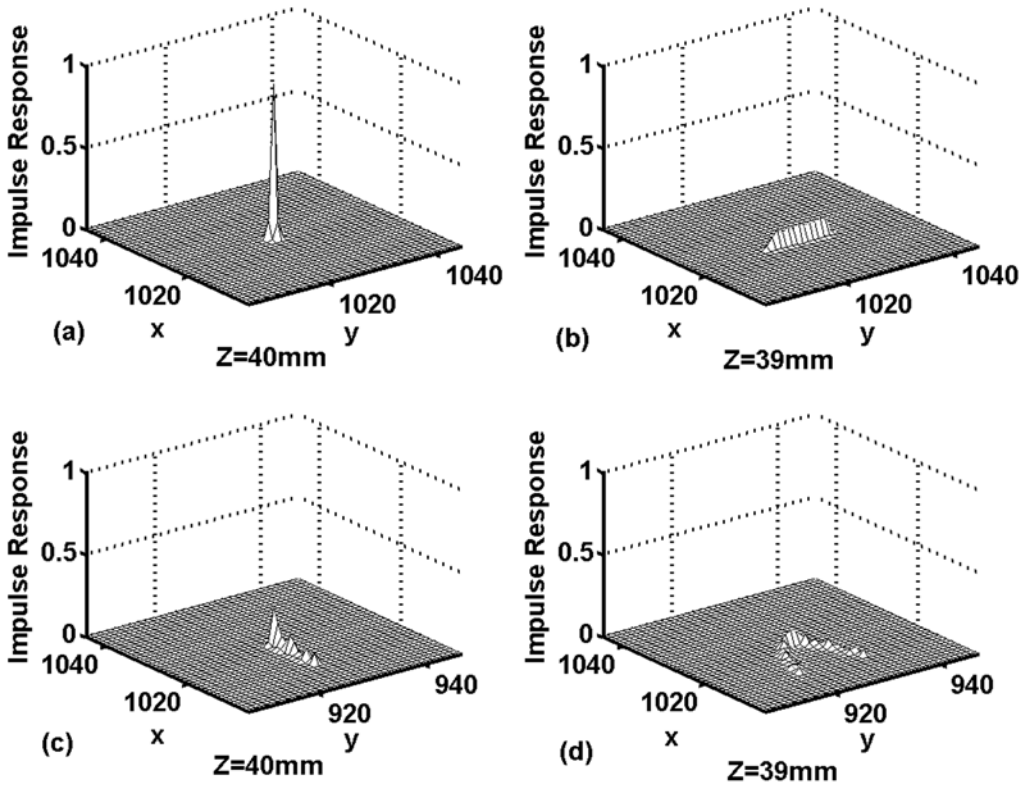

FIG. 3. Traditional SAA and point-by-point BP impulse responses: 25 projection images and 50^0 angular range, with the impulse located 40mm above the detector and about 4cm away from the chest wall. (a) and (b) give the impulse response of point-by-point BP; (c) and (d) give the impulse response of traditional SAA. (a) and (c) are impulse responses in the plane at the exact height of the impulse's location; (b) and (d) give corresponding values in a reconstruction plane 1mm below the impulse's location.

465

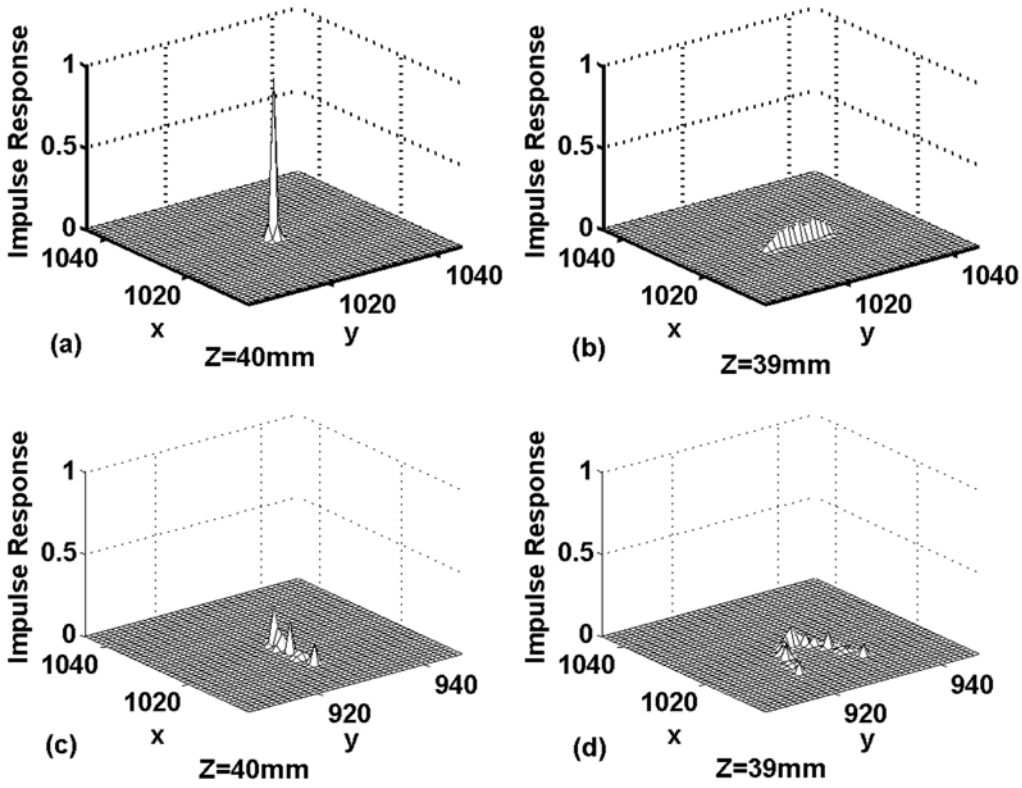

470

FIG. 4. Traditional SAA and point-by-point BP impulse responses: 13 projection images and 50^0 angular range, with the impulse located 40mm above the detector and about 4cm away from the chest wall. (a) and (b) give the impulse response of point-by-point BP; (c) and (d) give the impulse response of traditional SAA. (a) and (c) are impulse responses in
475 the plane at the exact height of the impulse's location; (b) and (d) give corresponding values in a reconstruction plane 1 mm below the impulse's location.

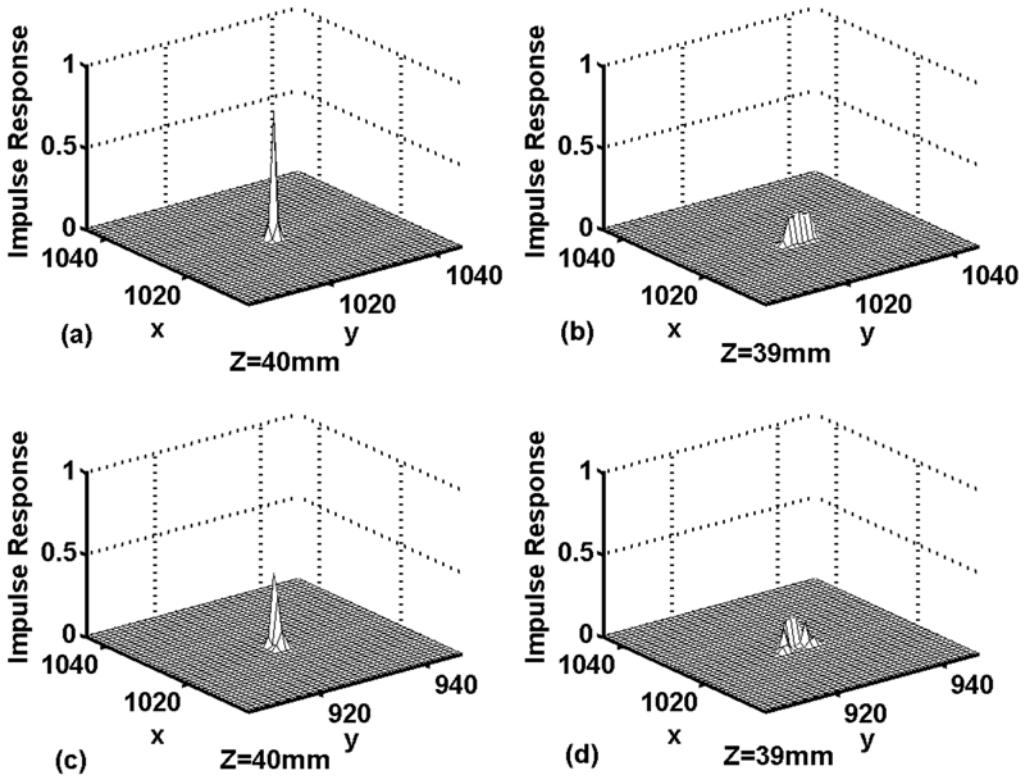

FIG. 5. Traditional SAA and point-by-point BP impulse responses: 25 projection images and 25^0 angular range, with the impulse located 40mm above the detector and about 4cm away from the chest wall. (a) and (b) give the impulse response of point-by-point BP; (c) and (d) give the impulse response of traditional SAA. (a) and (c) are impulse responses in the plane at the exact height of the impulse's location; (b) and (d) give corresponding values in a reconstruction plane 1 mm below the impulse's location.

485

Acquisition Parameters		Full Width at Tenth Maximum (in pixels)				Full Width at Half Maximum (in pixels)			
Projections	Total angular range	Traditional SAA		Point-by-point BP		Traditional SAA		Point-by-point BP	
		X axis	Y axis	X axis	Y axis	X axis	Y axis	X axis	Y axis
13	25^0	2.8	2.8	3.4	2.3	1.9	1.2	1.7	1.1
25	25^0	2.8	2.8	3.4	2.4	1.9	1.2	1.6	1.2
13	50^0	2.7	2.7	3.1	2.1	1.4	1.2	1.3	1.2
25	50^0	2.7	2.8	3.2	2.3	1.4	1.2	1.4	1.2
49	50^0	2.7	2.6	3.2	2.1	1.5	1.2	1.4	1.2

Table 1. The impulse is located near chest wall. Full width at half maximum (FWHM) and full width at tenth maximum (FWTM) measurements of in-plane impulse response
490 along two directions: tube's motion direction (Y axis) and direction orthogonal to tube's motion (X axis).

Acquisition Parameters		Full Width at Tenth Maximum (in pixels)				Full Width at Half Maximum (in pixels)			
Projections	Total angular range	Traditional SAA		Point-by-point BP		Traditional SAA		Point-by-point BP	
		X axis	Y axis	X axis	Y axis	X axis	Y axis	X axis	Y axis
13	25^0	3.7	2.8	2.8	2.5	2.0	1.2	1.2	1.2
25	25^0	3.6	2.8	2.6	2.3	2.0	1.2	1.2	1.2
13	50^0	11.8	2.5	2.2	2.1	(~13)* Multiple peaks	1.2	1.1	1.1
25	50^0	11.7	2.8	2.4	2.4	(~13)* Multiple peaks	1.2	1.2	1.2
49	50^0	11.4	2.8	2.6	2.1	(~13)* Multiple peaks	1.2	1.2	1.2

* For the 50^0 scan, multiple discrete peaks in the impulse response make FWHM not meaningful as a descriptor of impulse width. For these cases, the approximate overall width of the impulse is provided.

Table 2. The impulse is located 4 cm away chest wall. Full width at half maximum (FWHM) and full width at tenth maximum (FWTM) measurements of in-plane impulse response along two directions: tube's motion direction (Y axis) and direction orthogonal to tube's motion (X axis).

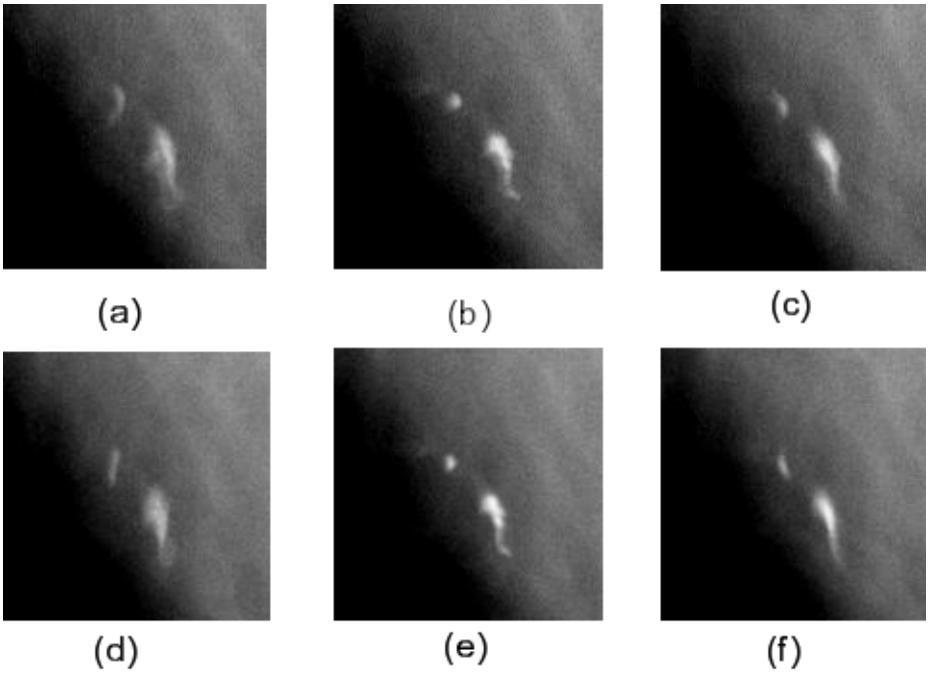

FIG.6. Reconstructed 12.75×12.75mm ROI of a human breast containing calcifications, Z=18 mm represents the plane height closet to the location of the calcification: (a) Traditional SAA, Z=16.5mm; (b) Traditional SAA, Z=18mm; (c) Traditional SAA, Z=19.5mm; (d) Point-by-point BP, Z=16.5mm; (e) Point-by-point BP, Z=18mm; (f) Point-by-point BP, Z=19.5mm

	Z=16.5mm			Z=18mm			Z=19.5mm		
	Shape	X width (in pixels)	Y width (in pixels)	Shape	X width (in pixels)	Y width (in pixels)	Shape	X width (in pixels)	Y width (in pixels)
Traditional SAA	curvilinear	10	21	punctate blurred	9	11	indistinct	11	16
Point-by-point BP	linear	7	20	punctate sharp	7	9	curvilinear	7	17

Table 3. Quantitative measurement of the leftmost calcification depicted in Fig. 6.

515

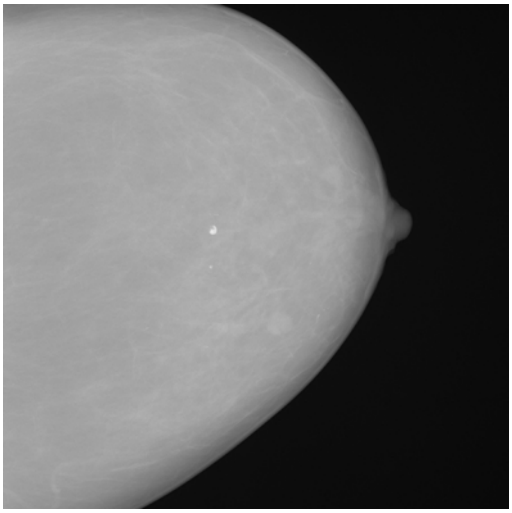

(a)

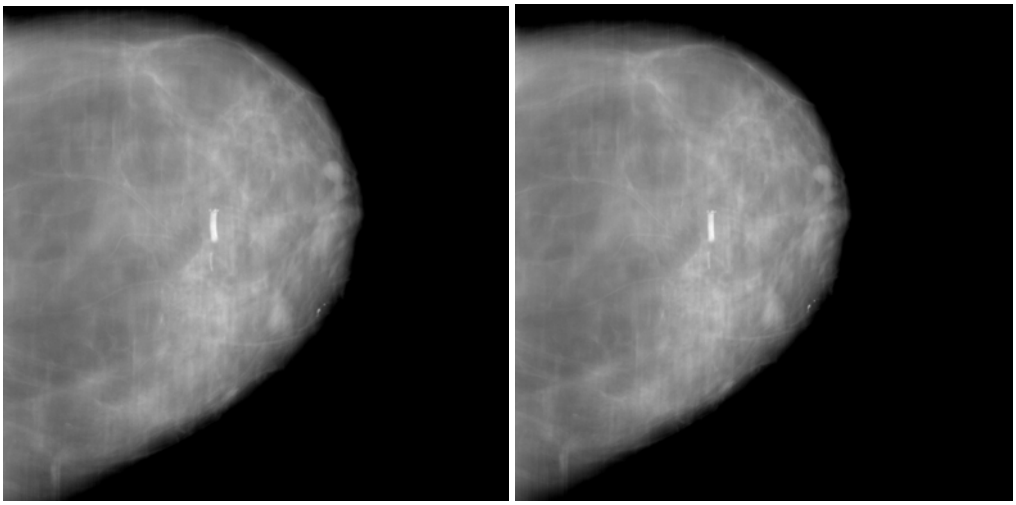

(b) (c)

FIG. 7. A human breast demonstrating a solitary calcification: (a) Low dose middle (0^0) projection image of the tomosynthesis sequence. The spectrum used for the tomosynthesis sequence was 28 kVp with W/Rh targer/filter and 112.5 mAs for a total of 25 projection images and 50^0 angular range. (b) Traditional SAA reconstructed slice image: Z=7.5mm. (c) Point-by-point BP reconstructed slice image: Z=7.5mm

REFERENCES

[1]L. W. Bassett, V. P. Jackson, K. L. Fu, Y. S. Fu, *Diagnosis of Diseases of the Breast,* 2nd ed. (Elsevier Saunders, Philadelphia, Pennsylvania, 2005).

[2]L. J. W. Burhenne, S. A. Wood, C. J. D'Orsi, S. A. Feig, D. B. Kopans, K. F. O'Shaughnessy, E. A. Sickles, L. Tabar, C. J. Vyborny, and R. A. Castellino, "Potential contribution of computer-aided detection to the sensitivity of screening mammography," Radiology **215**, 554-562 (2000).

[3]L.H. C. Burrell, D. M. Sibbering, A. R. Wilson, S. E. Pinder, A. J. Evans, L. J. Yeoman, C. W. Elston, I. O. Ellis, R. W. Blamey, and J. F. Tobertson, "Screening interval breast cancers: mammographic features and prognosis factors," AJR **199**, 811-817 (1996).

[4]A. M. Knutzen, and J. J. Gisvold, "Likelihood of malignant disease for various categories of mammographically detected, nonpalpable breast lesions," Mayo Clin Proc. **68**, 454-460 (1993).

[5]D. B. Kopans, "The positive predictive value of mammography," AJR, **158**, 521-526, (1992).

[6]J. T. Dobbins, III., D. J. Godfrey, "Digital X-ray tomosynthesis: current state of the art and clinical potential," Phys. Med. Biol. **48**, 65-106 (2003).

[7]Loren T. Niklason, et al., "Digital tomosynthesis in breast imaging," Radiology **205**, 399-406 (1997).

[8]Tao Wu, et al., "Tomographic mammography using a limited number of low-dose cone-beam projection images," Med. Phys. **30**, 365-380 (2003).

[9]Tao Wu, R. H. Moore, E. A. Rafferty, D. B. Kopans, "A comparison of reconstruction algorithms for breast tomosynthesis," Med. Phys. **9**, 2636-2647 (2004).

[10]S. Suryanarayanan, A. Karellas, S. Vedantham, S. J. Glick, C. J. D'Orsi, S. P. Baker, and R. L. Webber, "Comparison of tomosynthesis methods used with digital mammography," Acad. Radiol. **7**, 1085-1097 (2000).

[11]S. Suryanarayanan, A. Karellas, S. Vedantham, S. P. Baker, S. J. Glick, C. J. D'Orsi, S. P. Baker, and R. L. Webber, "Evaluation of linear and nonlinear tomosynthetic reconstruction methods in digital mammography," Acad. Radiol. **8**, 219-224 (2001).

[12]Y. Chen, J. Y. Lo, J. T. Dobbins III, "Impulse response analysis for several digital tomosynthesis mammography reconstruction algorithms," Proc. SPIE **5745**, 541-549 (2005).

[13]Y. Chen, J. Lo, J. T. Dobbins III, "Matrix Inversion Tomosynthesis (MITS) of the Breast: Preliminary Results," in *RSNA 90th Scientific Assembly*, Chicago, IL, 2004.

[14]Y. Chen, J. Y. Lo, J. A. Baker, J. T. Dobbins III, "Gaussian frequency blending algorithm with Matrix Inversion Tomosynthesis (MITS) and Filtered Back Projection (FBP) for better digital breast tomosynthesis reconstruction," Proc. SPIE **6142**, 122-130 (2006).

[15]Y. Chen, J. Y. Lo, J. A. Baker, J. T. Dobbins III, "Noise power spectrum analysis for several digital breast tomosynthesis reconstruction algorithms," Proc. SPIE **6142**, 1677-1684 (2006).

[16]X. Gong, S. J. Glick, B. Liu, A. A. Vedula, and S. Thacker, "A computer simulation study comparing lesion detection accuracy with digital mammography, breast tomosynthesis, and cone-beam CT breast imaging," Med. Phys. **33**, 1041-1052 (2006).

[17]G. M. Stevens, R. Fahrig and N. J. Pelc, “Filtered backprojection for modifying the impulse response of circular tomosynthesis,”.Med. Phys. **28**, 372-380 (2001).

[18]G. Lauritsch and W. Haerer, “A theoretical framework for filtered back-projection in tomosynthesis,” Proc. SPIE **3338**, 1127-1137 (1998).

[19]H. Matsuo, A. Iwata, I. Horiba, and N. Suzumura, “Three-dimensional image reconstruction by digital tomo-synthesis using inverse filtering,” IEEE Trans. Med. Imaging **12**, 307-313 (1993).

[20]T. Mertelemeier, J. Orman, W. Haerer, and M. K. Dudam, “Optimizing filtered backprojection reconstruction for a breast tomosynthesis prototype device,” Proc. SPIE **6142**, 131-142 (2006).

[21]M. Bissonnette, M. Hansroul, E. Masson, S. Savard, S. Cadieux, P. Warmoes, D. Gravel, J. Agopyan, B. T. Polischuk, W. H. Haerer, T. Mertelmeier, J. Y. Lo, Y. Chen, J. T. Dobbins III, J. L. Jesneck, S. Singh, “Digital breast tomosynthesis using an amorphous selenium flat panel detector,” Proc. SPIE **5745**, 529-540 (2005).

[22]B. Chen and R. Ning, “Cone-beam volume CT breast imaging,” Med. Phys. **29**, 755-770 (2002).

[23]A. Kak and M. Slaney, *Principles of Computerized Tomographic Imaging* (IEEE, New York, 1988).

[24]J. T. Dobbins, III, “Matrix Inversion Tomosynthesis improvements in longitudinal x-ray slice imaging (U.S. Patent #4,903,204),” Duke University, United States, 1990.

[25]D. J. Godfrey, R. L. Warp, J. T. Dobbins, III., “Optimization of matrix inverse tomosynthesis,” Proc. SPIE **4320**, 696-704 (2001).

[26]D. J. Godfrey, H. P. McAdams, and J. T. Dobbins, III, "Optimization of the matrix inversion tomosynthesis (MITS) impulse response and modulation transfer function characteristics for chest imaging," Med. Phys. **33**, 655 (2006).

[27]B. G. Ziedses des Plantes, "Eine neue methode zur differenzierung in der roentgenographie (planigraphie)," Acta Radiologica **13**, 182-192 (1932).

[28]A. D. Maidment, C. Ullberg, K. Lindman, L. Adelöw, J. Egerström, M. Eklund, T. Francke, U. Jordung, T. Kristoffersson, L. Lindqvist, D. Marchal, H. Olla, E. Penton, J. Rantanen, S. Solokov, N. Weber, and H. Westerberg, "Evalution of a photon-counting breast tomosynthesis imaging system," Proc. SPIE **6142**, 89-99 (2006).

[29]L. Zhou, J. Oldan, P. Fisher, and G. Gindi, "Low-contrast lesion detection in tomosynthetic breast imaging using a realistic breast phantom," Proc. SPIE **6142**, 1685-1696 (2006).

[30]L. A. Feldkamp, L. C. Davis, J. W. Kress, "Practical come-beam algorithm," J. Opt. Soc. Am. A **1**:612-619,1984.

[31]Y. Zhang, H. Chan, B. Sahiner, J. Wei, M. M. Goodsitt, L. M. Hadjiiski, J. Ge, C. zhou, "A comparative study of limited-angle cone-beam reconstruction methods for breast tomosynthesis," Med. Phys. 33(10), 3781-3795 (2006).

[32]J. T. Rakowski and M. J. Dennis, "A comparison of reconstruction algorithms for C-arm mammography tomosynthesis," Med. Phys. 33(8), 3018-3032 (2006).

[33]E. Samei, J. T. Dobbins III, J. Y. Lo, M. P. Tornai, "A framework for optimizing the radiographic technique in digital x-ray imaging," Radiation Protection Dosimetry (Oxford University Press, 2005).

TWO-DIMENSIONAL SHIFT-AND-ADD (SAA) ALGORITHM FOR DIGITAL BREAST TOMOSYNTHESIS RECONSTRUCTION

Introduction

Breast cancer is the most common cancer among women. Currently, mammography is the most important and efficacious tool for the early detection of breast cancer [7]. However, limitations of mammography have been well publicized, such as 20% false negative rate [8, 9], many callbacks from screening, and low positive predictive value of about 15-34% from biopsy [10, 11]. It is very difficult for conventional two-dimensional mammography to distinguish a cancer from overlying breast tissues.

Digital breast tomosynthesis is a three-dimensional imaging technique that provides an arbitrary set of reconstruction planes in the breast from limited-angle series of projection images when x-ray tube moves [1-5]. Shift-And-Add (SAA) tomosynthesis reconstruction algorithm is a common mathematical method to line up each projection image based on its shifting amount to generate the reconstruction slices. Various efforts have been made on SAA reconstruction for breast imaging [1,2,3,5]. However, among those efforts, shift amounts for each projection plane was calculated only along the axis of x-ray tube's movement. This brings inaccuracy to the reconstructed slice images. This project aims to investigate a two-dimensional correction for the SAA algorithm to correctly calculate the shift amount based on isocentric tube motion, in order to generate more accurate and reliable reconstruction images.

Methods and Materials

A. Breast tomosynthesis system

A selenium-based direct conversion Siemens Mammomat Novation prototype system with the pixel size of 85 μm was used as the breast tomosynthesis acquisition system. It can generate tomosynthesis sequences of up to 49 projection images with a total angular range of 0-50 degrees. A few tomosynthesis sequences of human subjects were acquired for investigation and comparison.

B. Two-dimensional SAA algorithm

In order to reconstruct slice images of the breast, each projection image should be lined up based on the shift amount appropriate for the plane of reconstruction. The shift amount of each projection image was calculated according to the relative positions of the projection image and geometric parameters of the tomosynthesis acquisition system. In-focus structures in a given plane were lined up for reconstruction.

During tomosynthesis sequence acquisition, the x-ray tube moves above the chest wall along an arc. Figure 1 shows the arc path of motion when x-ray tube moves along x axis. Point P represents a single structure on a certain reconstruction plane. P_1, P_2, P_3 are the actual projected locations of point P on the detector for different x-ray tube locations of A_1, A_2, A_3 specifically. The actual path of the projected location follows a two-dimensional arc rather than a one-dimensional line. However, with the traditional Shift-And-Add (SAA) algorithm for breast tomosynthesis reconstruction, shift amounts for each projection plane are calculated only along one axis of x-ray tube's movement. As a result, small objects such as microcalcifications appear slightly blurred in the direction perpendicular to the direction of tube motion.

Because of the isocentric motion of the x-ray tube, the shift amount occurs at both x and y two-dimensional directions on each projection image. For our two-dimensional SAA method, shift amounts for every pixel location on each reconstruction plane were computed, taking into account the 2D arc projection location of reconstructed objects in each plane. Bilinear interpolation was used for partial pixel locations.

C. Impulse response analysis

Impulses at different 3-D locations were simulated to investigate the sharpness of reconstructed in-plane structures and the effectiveness at removing out-of-plane blur. Datasets with 49, 25 and 13 projection images of the impulse were generated with a total angular movement of 25 and 50 degrees of the simulated x-ray point source. Four groups of impulses were simulated: 1) impulse that is exactly underneath the x-ray source (near the chest wall) and in a defined reconstructed plane; 2) impulse that is exactly underneath the x-ray source (near the chest wall) and halfway between reconstructed planes; 3) impulse that is approximately 4 cm away from the chest wall and in a defined reconstructed plane; 4) impulse that is approximately 4 cm away from the chest wall and halfway between reconstructed planes. The impulse response in the spatial domain was analyzed for evaluation.

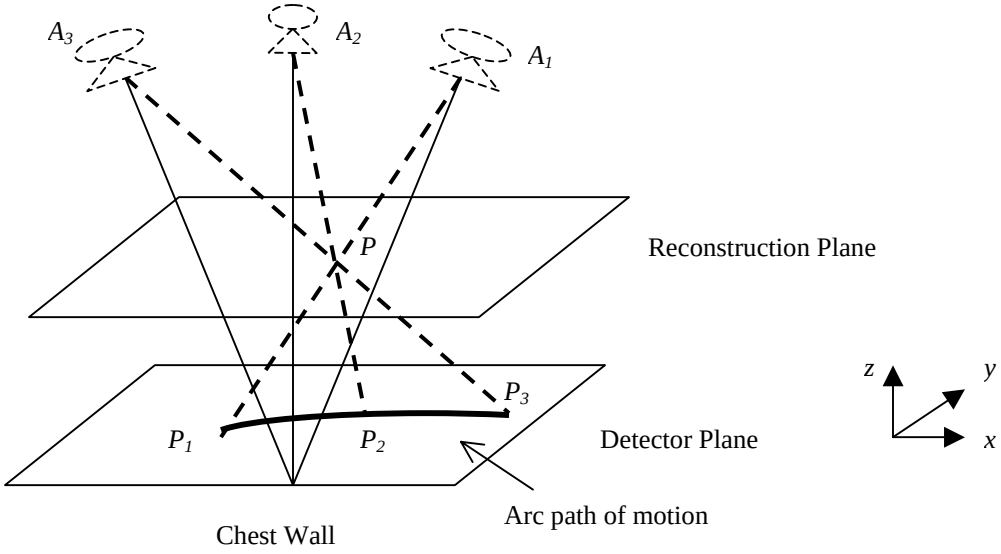

Figure 1. Arc path of motion when x-ray tube moves along *x* axis

Results

According to impulse response analysis, two-dimensional SAA demonstrated the improvement in the direction that is perpendicular to the tube motion direction. According to human subjects results, the appearance of calcifications from two-dimensional SAA was sharper than traditional SAA at the direction orthogonal to the tube motion direction. Out-of-plane artifacts of calcifications changed from curved to be straight.

Figure 2 shows two reconstruction slices for a human subject. Figure 3 shows reconstructed ROI images of the same human subject. The tomosynthesis sequence was acquired with 25 projections and $+/-25^0$angular range, with a total exposure of 1.5 times of a single CC view. Figure 3(a), (b) are reconstructed ROIs of a calcification on a single slice from traditional SAA and 2D SAA specifically. We can find that the appearance of calcifications from two-dimensional SAA was sharper and more accurately defined. Figure 3(c), (d) show the out-of-plane blur of a calcification. Out-of-plane artifacts of calcifications changed from curved to be straight after 2D SAA.

We also found that, when x-ray tube moves above the breast along an arc, for different locations of structures on a single reconstruction plane, the magnification difference existed. This is more substantial for structures further away from the chest wall. Two-dimensional SAA correctly addressed this issue by calculating shift amounts for every pixel location on each reconstruction plane.

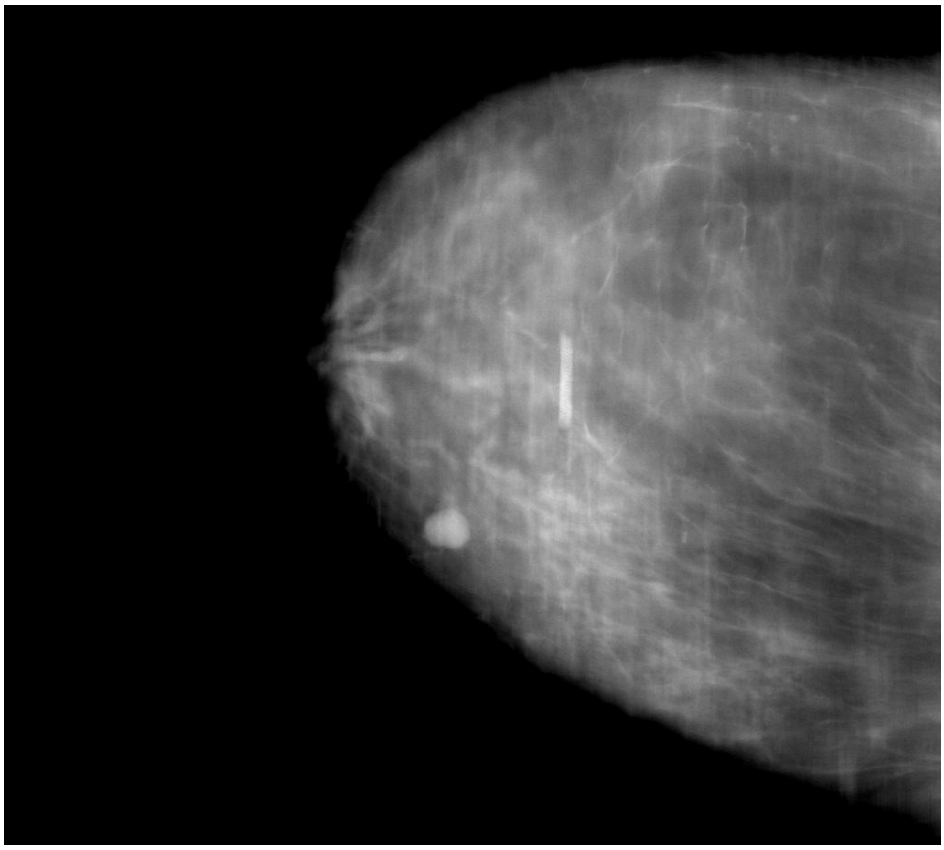

Figure 2(a).
2D SAA:
Single reconstruction slice
with mass on it

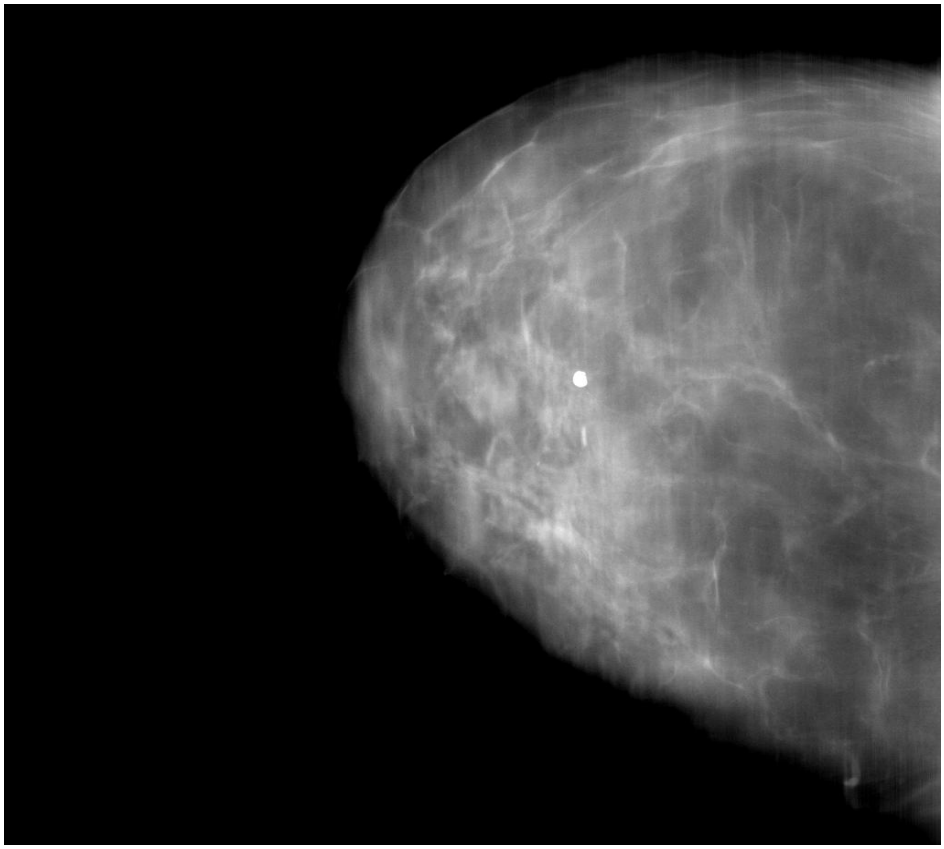

Figure 2(b).
2D SAA:
Single reconstruction slice
with big calcification on it

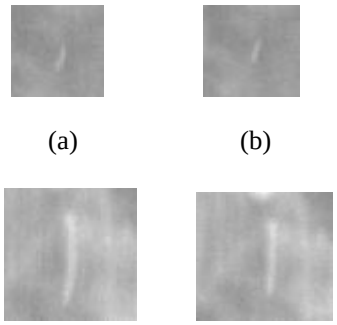

(a) (b)

(c) (d)

Figure 3. Reconstructed ROI of a human subject:

(a) Traditional SAA: calcification
(b) Two-dimensional SAA: calcification
(c) Traditional SAA: out-of-plane blur of calcification
(d) Two-dimensional SAA: out-of-plane blur of calcification

Conclusions

This work demonstrates that the two-dimensional SAA is an effective method to reconstruct 3D tomosynthesis images of the breast. Compared with the traditional SAA algorithm, the new method corrects for two-dimensional shift amounts coming from the isocentric x-ray tube's movement. This provides more accurate and reliable results than other SAA algorithms.

The two-dimensional SAA does appear to improve the sharpness and morphology of calcifications. However, it is not spatially invariant method, therefore may be more difficult to be used with linear deblurring techniques.

Acknowledgements

This work was supported in part by a research grant from Siemens.

References

1. James T. Dobbins, III., Devon J. Godfrey, "Digital X-ray tomosynthesis: current state of the art and clinical potential", Phys. Med. Biol. 48: R65-R106, 2003.
2. Ying Chen, Joseph Y. Lo, James T. Dobbins III, "Impulse response analysis for several digital tomosynthesis mammography reconstruction algorithms", Proc. SPIE, Volume 5745, Physics of Medical Imaging, pp 541-549, 2005.
3. Ying Chen, Joseph Y. Lo, James T. Dobbins III, "Noise power spectrum analysis for several digital breast tomosynthesis reconstruction algorithms", Proc. SPIE, Physics of Medical Imaging, 2006.
4. Michel Bissonnette, Marc Hansroul, Eric Masson, Serge Savard, Sébastien Cadieux, Patrick Warmoes, Daniel Gravel, Jerry Agopyan, Brad T. Polischuk, Wolfgang H. Haerer, Thomas Mertelmeier, Joseph Y. Lo, Ying Chen, James T. Dobbins III, Jonathan L. Jesneck, Swatee Singh, "Digital breast tomosynthesis using an amorphous selenium flat panel detector", Proc. SPIE, Volume 5745, Physics of Medical Imaging, pp 529-540, 2005.
5. Loren T. Niklason, et al., "Digital tomosynthesis in breast imaging", Radiology 205: 399-406, 1997.
6. B. G. Ziedses des Plantes, "Eine neue methode zur differenzierung in der roentgenographie (planigraphie). Acta Radiologica", 13: 182-192, 1932.
7. Lawrence W. Bassett, Valerie P. Jackson, Karin L. Fu, Yao S. Fu, "Diagnosis of Diseases of the Breast", 2nd ed, Elsevier Saunders, Philadelphia, Pennsylvania, 2005.
8. L. J. W. Burhenne, S. A. Wood, C. J. D'Orsi, S. A. Eeig, D. B. Kopans, K. F. O'Shaughnessy, E. A. Sickles, L. Tabar, C. J. Vyborny, and R. A. Castellino, "Potential contribution of computer-aided detection to the sensitivity of screening mammography", Radiology, 215:554-562, 2000.
9. H. C. Burrell, D. M. Sibbering, A. R. Wilson, S. E. Pinder, A. J. Evans, L. J. Yeoman, C. W. Elston, I. O. Ellis, R. W. Blamey, and J. F. Tobertson, "Screening interval breast cancers: mammographic features and prognosis factors", AJR, 199:811-817, 1996.
10. A. M. Knutzen, and J. J. Gisvold, "Likelihood of malignant disease for various categories of mammographically detected, nonpalpable breast lesions", Mayo Clin Proc, 68:454-460, 1993.
11. D. B. Kopans, "The positive predictive value of mammography", AJR, 158:521-526, 1992.

Methodology of NEQ (f) analysis for optimization and comparison of digital breast tomosynthesis acquisition techniques and reconstruction algorithms

Ying Chen[a,b], Joseph Y. Lo[a,b,c,d], Nicole T. Ranger[b,c], Ehsan Samei[a,b,c,d], James T. Dobbins III[a,b,c,d]

[a]Department of Biomedical Engineering, Duke University, Durham, NC, USA 27710
[b]Duke Advanced Imaging Laboratories, Duke University Medical Center, Durham, NC, USA 27710
[c]Department of Radiology, Duke University Medical Center, Durham, NC, USA 27710
[d]Medical Physics Graduate Program, Duke University Medical Center, Durham, NC, USA 27710

ABSTRACT

As a new three-dimensional imaging technique, digital breast tomosynthesis allows the reconstruction of an arbitrary set of planes in the breast from a limited-angle series of projection images. Though several tomosynthesis algorithms have been proposed, no complete optimization and comparison of different tomosynthesis acquisition techniques for available methods has been conducted as of yet. This paper represents a methodology of noise-equivalent quanta NEQ (f) analysis to optimize and compare the efficacy of tomosynthesis algorithms and imaging acquisition techniques for digital breast tomosynthesis. It combines the modulation transfer function (MTF) of system signal performance and the noise power spectrum (NPS) of noise characteristics. It enables one to evaluate the performance of different acquisition parameters and algorithms for comparison and optimization purposes. An example of this methodology was evaluated on a selenium-based direct-conversion flat-panel Siemens Mammomat Novation prototype system. An edge method was used to measure the presampled MTF of the detector. The MTF associated with the reconstruction algorithm and specific acquisition technique was investigated by calculating the Fourier Transform of simulated impulse responses. Flat field tomosynthesis projection sequences were acquired and then reconstructed. A mean-subtracted NPS on the reconstructed plane was studied to remove fixed pattern noise. An example of the application of this methodology was illustrated in this paper using a point-by-point Back Projection correction (BP) reconstruction algorithm and an acquisition technique of 25 projections with 25 degrees total angular tube movement.

Keywords: mammography, tomosynthesis, breast imaging, modulation transfer function (MTF), noise power spectrum (NPS), Noise-equivalent quanta (NEQ), impulse response, Back Projection (BP)

1. INTRODUCTION

Digital breast tomosynthesis is a new technique to reconstruct an arbitrary set of planes in the breast from a limited-angle series of projection images when the x-ray source moves along an arc above the breast. As of yet, several tomosynthesis algorithms have been proposed [3,4,10-22], including Shift-And-Add (SAA) [3,4], Niklason and colleagues' publication in 1997 of a tomosynthesis method with the x-ray tube moved in an arc above the stationary breast and detector [10], Wu et al.'s report in 2003 of the maximum likelihood iterative algorithm (MLEM) to reconstruct the three-dimensional distribution of x-ray attenuation in the breast [11], and the filtered back projection (FBP) algorithms [12,13,18-24], tuned-aperture computed tomography (TACT) reconstruction methods developed by Webber and investigated by Suryanarayanan *et al*[16], algebraic reconstruction techniques (ART) [14.23.24], filtered back projection (FBP) [4,13,18-21], matrix inversion tomosynthesis (MITS) [15,26] and Gaussian Frequency Blending (GFB) algorithm to combine the MITS and FBP for better reconstruction [22].

The selection of optimal acquisition parameters and reconstruction algorithm plays an important role in producing better performance. However, there are several factors involved in this task and some of them are not individually independent. An effective methodology will enable one to optimize selection of acquisition parameters and compare algorithms for various digital breast tomosynthesis methods. Recently, Godfrey et al. proposed methods of MTF and NPS measurement to quantitatively characterize the optimal acquisition parameters selection for chest tomosynthesis application [6,7]. In 2005 and 2006, we also published the impulse response and NPS analysis for different acquisition parameters and reconstruction algorithms [3,4].

In this paper, a methodology of NEQ (f) analysis is proposed to optimize and compare the efficacy of tomosynthesis algorithms and imaging acquisition techniques for digital breast tomosynthesis. It combines the modulation transfer function (MTF) of system signal performance and the noise power spectrum (NPS) of noise characteristics. It enables one to evaluate the performance of different acquisition parameters and algorithms for comparison and optimization purposes.

2. METHODS

The NEQ (f) is defined as: $NEQ(f) = \frac{MTF^2(f)}{NNPS(f)}$. The modulation transfer function (MTF) and the normalized noise power spectrum (NNPS) are included to evaluate the performance of the reconstruction algorithms and the acquisition techniques. The normalized NPS (NNPS) is defined as: $NNPS(u,v) = \frac{NPS_{tomo}(u,v)}{gain^2}$ due to the logarithmic transform in digital tomosynthesis. Hence, the NEQ (f) can be calculated by: $NEQ(f) = \frac{gain^2 \cdot MTF^2(f)}{NPS_{tomo}(f)}$. In digital breast tomosynthesis reconstruction, the step of logarithmic transform involved, and therefore, the determination of NEQ (f) is more similar to that of a screen-film system than to a linear digital detector.

2.1 MTF measurement

The MTF measurement includes two parts: 1) the system MTF of the detector; 2) the reconstruction MTF associated with specific reconstruction algorithm and acquisition parameters.

2.1.1 System MTF Measurement

The system MTF describes the measured MTF of the detector. An edge method was applied at a range of tube angles to see if there is any difference with angle. In this paper, five different angular positions of 0^0, $\pm 15^0$, and $\pm 25^0$ of the X-ray tube were selected as the representative angles.

Table 1 shows the MW2 [8] technique we used for the system MTF measurement.

Technique	Acquisition Mode	kV	Spectrum	Number of views (N)	Total mAs	mAs for a single projection
MW2	B0XD11 (slow speed)	28	W/Rh	11	303	≈ 27.5

Table 1. System MTF measurement technique

Figure 1 shows the set up of the system MTF measurement experiment. A 0.1mm Pt-Ir edge was placed in contact with the detector and oriented at a $1^0 \sim 3^0$ angle with respect to the pixel array. Edge images were then acquired with MW2 technique and 2mm Aluminum filtration. A previously published routine [8,9] was used to analyze the edge images in a region around the edge (ROI=256*256 pixels, pixel size=85μm) to compute the presampled system MTF.

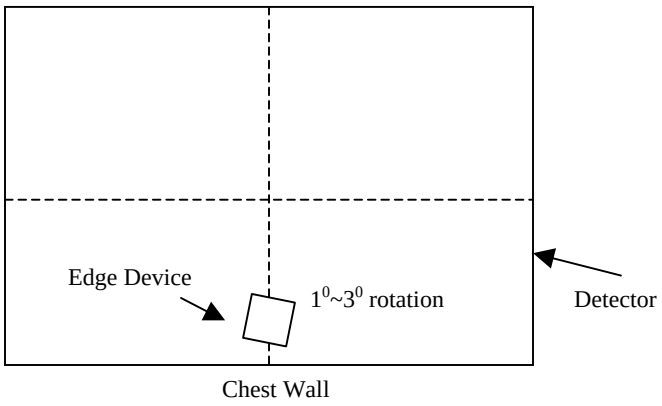

Figure 1. Set up of system MTF measurements

2.1.2 Reconstruction MTF measurement

The reconstruction MTF describes the calculated MTF associated with specific algorithm and acquisition parameters. A dataset of tomosynthesis projection images of a simulated delta function with the specific acquisition parameters was served as the input signal. A ray-tracing simulation method was used to project the single delta function onto the detector to simulate the tomosynthesis sequence of projection images. Figure 2 shows the ray-tracing method to simulate the projection images of a delta function.

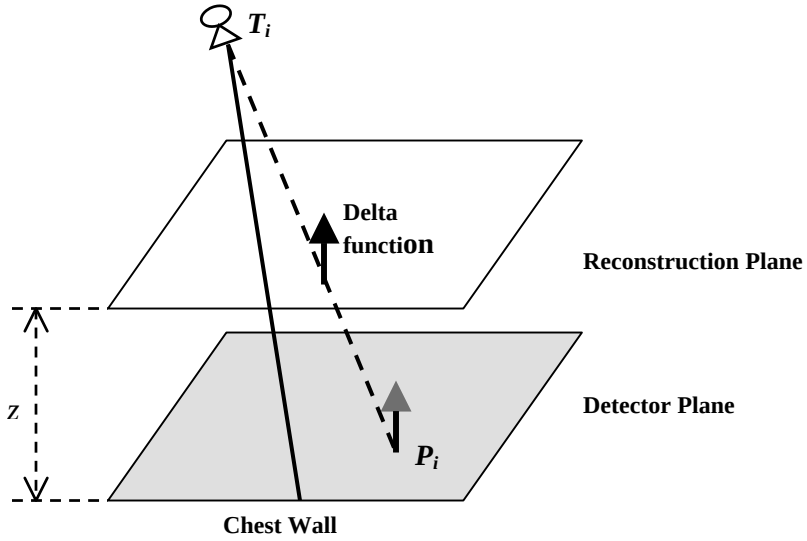

Figure 2. Ray-tracing simulation

In Figure 2, a single delta function at *z* distance above the detector was simulated. The delta function is projected onto the detector at P_i when the x-ray tube moves to T_i location. Partial pixel sharing was performed if P_i falls into non-integer pixel location. With this ray-tracing method, for a specific group of acquisition parameters, a dataset of projection images from different x-ray tube locations can be simulated.

Projection images with $1/r^2$ background and without background were considered, where r is the distance between the x-ray source T_i and the pixel location P_i on each projection image. Datasets of simulated projection images with $1/r^2$ background and without background were separately reconstructed by the specific reconstruction algorithm. The reconstruction images without background were then subtracted from the reconstruction images with background to get rid of effects associated with the $1/r^2$ background ray-tracing simulation.

The reconstruction MTF can be computed as the Fourier Transform of the point spread function (PSF) on the reconstruction plane where the simulated delta function is located (z distance above the detector).

2.1.3 Total MTF

The total MTF involves two parts as described in 2.1.1 and 2.1.2. It can be calculated as the multiplication of measured system MTF (2.1.1) and the reconstruction MTF associated with reconstruction algorithm and acquisition parameters (2.1.2). Linear interpolation was performed to match the frequency axes of the system MTF and reconstruction MTF for multiplication.

2.2 NPS measurement

In order to compute the noise power spectrum (NPS) for specific acquisition parameters, two phantom slabs of BR12 (47% water/ 53% adipose equivalent) for a total of 4 cm thickness were put directly on the detector cover to mimic the breast tissue equivalent attenuation and scattered radiation. Ten identical tomosynthesis sequences of flat images with the phantom slabs on the detector were acquired. The tomosynthesis sequences were then reconstructed.

Mean-subtracted reconstruction image data were analyzed and compared on a reconstruction plane with the same height (z distance above the detector) as described in the reconstruction MTF measurement (2.1.2). The purpose of studying mean-subtracted NPS is to remove fixed pattern noise, including structured noise and system artifacts. A previously published method [1,2] was applied using 64 ROIs of size 128×128 to examine the noise response.

2.3 Gain factor calculation

In order to normalize NPS and fairly compare different reconstruction algorithms and acquisition parameters, the gain factor should be included in the NEQ (f) calculation.

For an x-ray screen-film imaging system, the gain factor can be considered as $gain = \log_{10}(e) \cdot \gamma$, where γ is the point slope of the film density-log x-ray fluence function [28,29]. Figure 3 shows a typical screen-film nonlinear response to exposure. Q represents the number of incident quanta / mm^2. From this nonlinear response curve, one can calculate the point slope γ for a specific $log(Q)$ on this response curve.

With digital tomosynthesis, the gain factor varies with different reconstruction algorithms and acquisition techniques. In this paper, we focus on the relative NEQ (f) methodology of a single algorithm and will not include the gain factor calculation. The gain factor will be computed in future work where we will actually compare different algorithms against one another.

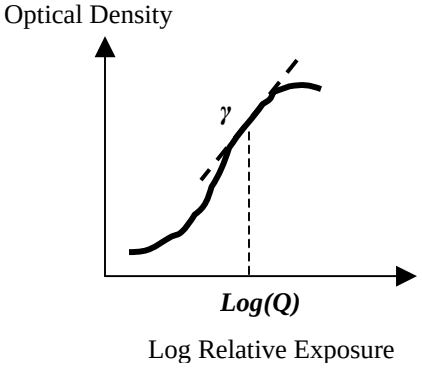

Figure 3. Screen-film characteristic curve

2.4 NEQ (f) calculation

The NEQ (f) can be calculated by: $NEQ(f) = \frac{gain^2 \cdot MTF^2(f)}{NPS_{tomo}(f)}$. After measuring the MTF, NPS and gain factor, one can combine them together to get the NEQ (f) result. Linear interpolation was performed to match the frequency axes of the NPS and MTF curves. In this paper, the relative NEQ (f) along two directions were investigated separately, including the x-ray tube's movement direction and the direction orthogonal to tube's motion direction.

3. RESULTS

Here we give an example of NEQ (f) measurement. A prototype Siemens system with 85μm pixel size was used. A point-by-point Back Projection (BP) reconstruction algorithm [27] was investigated. Compared with traditional shift-and-add, point-by-point BP algorithm demonstrates improved rendition of microcalcifications in the direction perpendicular to the tube motion direction, thus provides sharper appearance of calcifications with human subject images [27].

A data set of tomosynthesis projection images of a delta function at 40 mm above the detector surface plate and 40 mm away the chest wall was simulated with acquisition parameters of 25 projection images and 25 degrees of total angular range of tube movement. The simulated tomosynthesis sequence was reconstructed by point-by-point BP. Figure 4 shows the impulse and MTF results on the reconstruction plane of the delta function's location (40 mm above the detector). In figure 4(a), x and *y* axes represents the pixel location on the image. In figure 4(b), the v axis represents the spatial frequency conjugate to the direction of tube's motion direction.

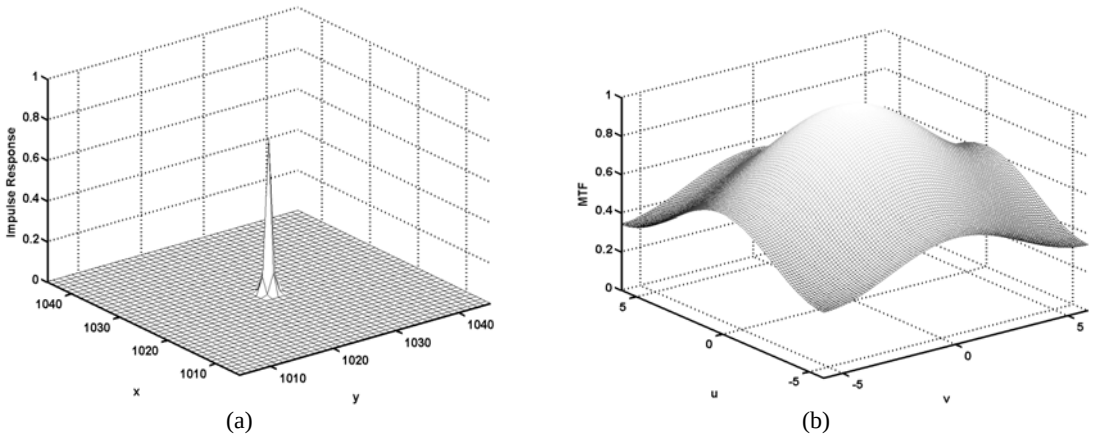

(a) (b)

Figure 4. Point-by-point BP with 25 projections and $\pm 15^0$ total angular range: (a) impulse response; (b) MTF

We find that the point-by-point BP is an effective reconstruction method for digital breast tomosynthesis. The MTF curve is smooth and the impulse response appears to be sharp at the reconstruction plane where the simulated delta function is located (figure 4).

Figure 5 shows the edge-method measured system MTF when the edge center was about 4cm away from the chest wall and the X-ray tube was at angles of 0^0, $\pm 15^0$, $\pm 25^0$. Three datasets were measured and averaged for each angular location of the x-ray tube. The MTF varied little with different angles. The MTF curve of -25^0 is a little lower than that of other angles. This may be caused by x-ray tube's motion and velocity difference at the -25^0 location, which is the beginning position of the x-ray tube during the tomosynthesis sequence.

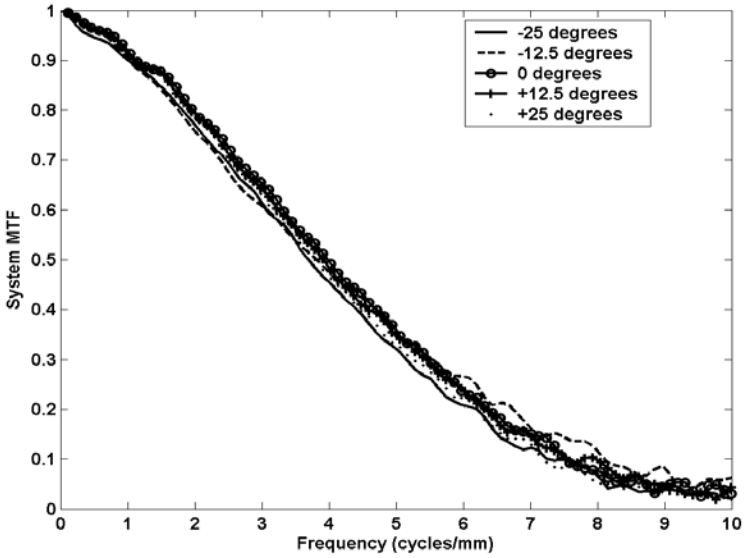

Figure 5. System MTF at different angles by edge method measurement

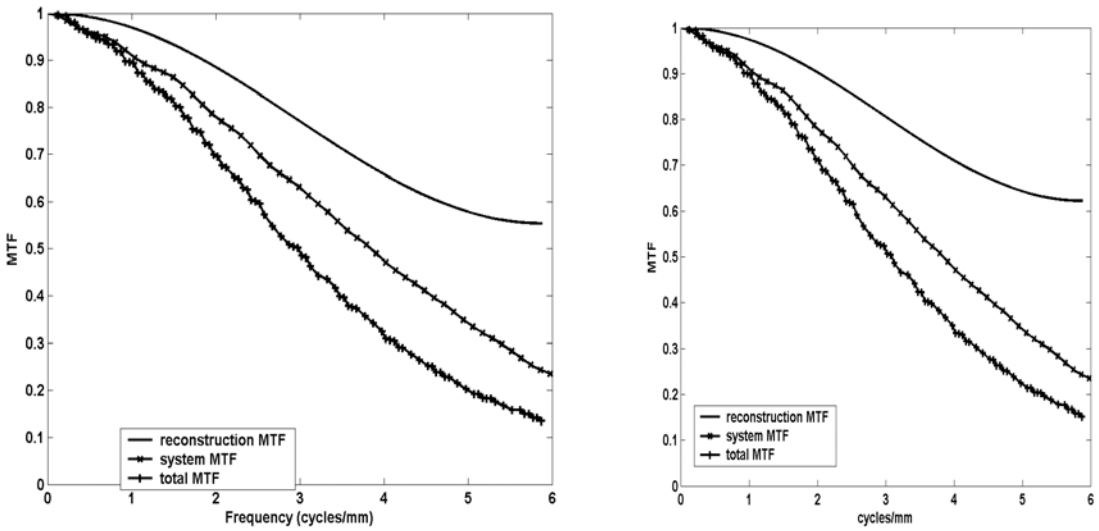

(a) (b)

Figure 6. Reconstruction, system, and total MTFs: (a) direction orthogonal to tube's motion direction (b) tube's motion direction

Figure 6 shows the averaged system MTF, reconstruction MTF (point-by-point BP algorithm, 25 projection images and $\pm 12.5^0$ total tube angular movement), and the total MTF as the multiplication of above two MTFs. The reconstruction MTF is much higher than the system MTF.

For measurement of NPS, a W/Rh spectrum and 28 KV were used with a cumulative tube output of 358 mAs. Mean-subtracted NPS of reconstructed planes at the same location of 40mm above the detector surface plate was computed as shown in figure 7. Figure 8 shows the relative NEQ (f) results without gain factor calculation. Further theoretical and experimental studies will be done to investigate the gain factor for each reconstruction algorithm and

acquisition technique. Results along both tube's movement direction and direction orthogonal to the tube's motion are shown in figures 7 and 8. The NPS and relative NEQ (f) performances along both directions were similar.

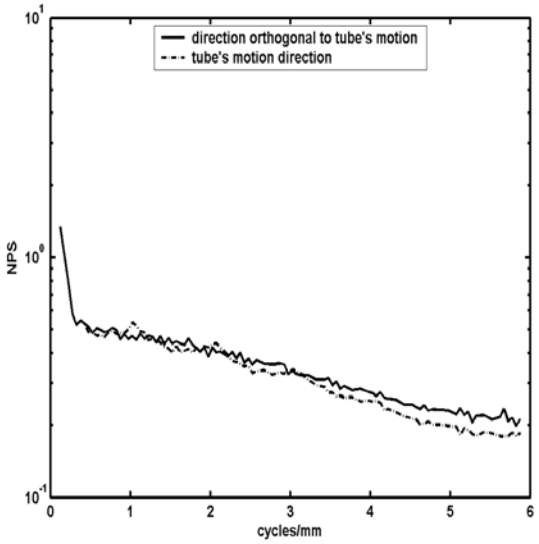

Figure 7. Mean-subtracted NPS

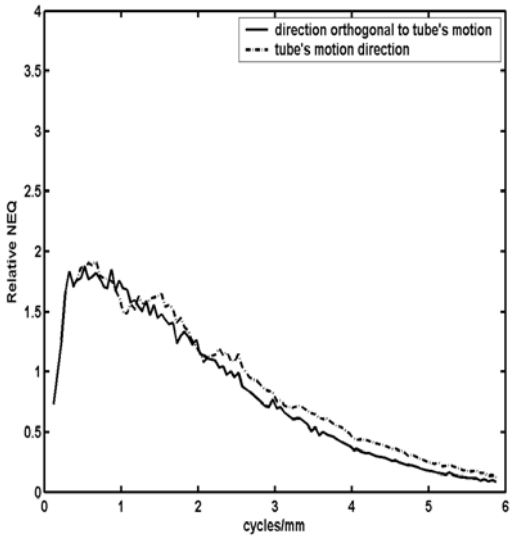

Figure 8. Relative NEQ (f)

4. CONCLUSION

The NEQ (f) is an image quality metric that combines both signal and noise properties to compare different acquisition techniques and reconstruction algorithms in tomosynthesis. In this paper, MTF and NPS were evaluated by experiments, simulation, and the application of several published routines. This provides empirical results for comparing and selecting optimal tomosynthesis acquisition parameters and reconstruction algorithms, and enables elucidation of imaging geometry factors in directions parallel and orthogonal to tube motion.

ACKNOWLEDGMENTS

We thank Jay A. Baker, M.D., at Duke University Medical Center for clinical insight and helpful discussion. This work was supported in part by a research grant from Siemens Medical Solutions and a grant from US Army Breast Cancer Research Program (USAMRMC W81XWH-06-1-0462).

REFERENCE

1. J. T. Dobbins III, D.L. Ergun, L. Rutz, D. A. Hinshaw, H. Blume, D. c. Clark, "DQE (f) of four generations of comouted radiography acquisition devices", *Med. Phys. 22 (10): 1581-1593 (1995).*
2. J. T. Dobbins III, "Image quality metrics for digital systems," *in Handbook of Medical Imaging, edited by H .K.J. Beutel and R. V. Metter (SPIE, Washington, D.C., 2000), Vol. 1, pp. 163-222.*
3. J. T. Dobbins, III., D. J. Godfrey, "Digital X-ray tomosynthesis: current state of the art and clinical potential", *Phys. Med. Biol. 48: R65-R106 (2003).*
4. Y. Chen, J. Y. Lo, J. T. Dobbins III, "Impulse response analysis for several digital tomosynthesis mammography reconstruction algorithms," *Proc. SPIE 5745, 541-549 (2005).*
5. Y. Chen, J. Y. Lo, J. A. Baker, J. T. Dobbins III, "Noise power spectrum analysis for several digital breast tomosynthesis reconstruction algorithms," *Proc. SPIE 6142, 1677-1684 (2006).*
6. D. J. Godfrey, H. P. McAdams, J. T. Dobbins III, "Stochastic noise characteristics in matrix inversion tomosynthesis (MITS)," submitted manuscript.
7. D. J. Godfrey, H. P. McAdams, J. T. Dobbins III, "Optimization of the Matrix Inversion Tomosynthesis (MITS) impulse response and modulation transfer function characteristics for chest imaging," *Med. Phys. 33(3), 655-667 (2006).*
8. R. S. Saunders, E. Samei, J. Jesneck, J. Lo, "Physical characterization of a prototupe selenium-based full field digital mammography detector," *Med. Phys. 32(2), 588-599 (2005).*
9. R. S. Saunders and E. Samei, "A method for modifying the image quality parameters of digital radiographic images," *Med. Phys. 30, 3006-3017 (2003).*
10. L. T. Niklason, et al., "Digital tomosynthesis in breast imaging", *Radiology 205: 399-406 (1997).*
11. Tao Wu, et al., "Tomographic mammography using a limited number of low-dose cone-beam projection images", Med. Phys. 30 (3): 365-380, March 2003.
12. T. Wu, R. H. Moore, E. A. Rafferty, D. B. Kopans, "A comparison of reconstruction algorithms for breast tomosynthesis", *Med. Phys. 9: 2636-2647 (2004).*
13. T. Mertelemeier, J. Orman, W. Haerer, and M. K. Dudam, "Optimizing filtered backprojection reconstruction for a breast tomosynthesis prototype device," Proc. SPIE 6142, 131-142 (2006).
14. Y. Zhang, H. Chan, B. Sahiner, J. Wei, M. M. Goodsitt, L. M. Hadjiiski, J. Ge, C. Zhou, "A comparative study of limited-angle cone-beam reconstruction methods for breast tomosynthesis," Med. Phys. 33(10), 3781-3795 (2006).
15. Y. Chen, J. Lo, J. T. Dobbins III, "Matrix Inversion Tomosynthesis (MITS) of the Breast: Preliminary Results", RSNA 90th Scientific Assembly, Chicago, IL, 2004.
16. S. Suryanarayanan, A. Karellas, S. Vedantham, S. J. Glick, C. J. D'Orsi, S. P. Baker, and R. L. Webber, "Comparison of tomosynthesis methods used with digital mammography," Acad. Radiol. 7, 1085-1097 (2000).
17. A. D. Maidment, C. Ullberg, K. Lindman, L. Adelöw, J. Egerström, M. Eklund, T. Francke, U. Jordung, T. Kristoffersson, L. Lindqvist, D. Marchal, H. Olla, E. Penton, J. Rantanen, S. Solokov, N. Weber, and H. Westerberg, "Evalution of a photon-counting breast tomosynthesis imaging system," Proc. SPIE 6142, 89-99 (2006).
18. D. G. Grant, "Tomosynthesis: a three-dimensional radiographic imaging technique", IEEE Transactions on Biomedical Engineering. BME-19: 20-28, 1972
19. Grant M. Stevens, Rebecca Fahrig and Norbert J. Pelc, "Filtered backprojection for modifying the impulse response of circular tomosynthesis", Med. Phys. 28: 372-380, 2001.
20. G. Lauritsch and W. Haerer, "A theoretical framework for filtered back-projection in tomosynthesis", Proc. SPIE 3338: 1127-1137, 1998.
21. Hiroshi Matsuo, Akira Iwata, Isao Horiba, Nobuo Suzumura, "Three-dimensional image reconstruction by digital tomo-synthesis using inverse filtering", IEEE Trans. Med. Imaging. 12: 307-313, 1993.
22. Y. Chen, J. Y. Lo, J. A. Baker, J. T. Dobbins III, "Gaussian frequency blending algorithm with Matrix Inversion Tomosynthesis (MITS) and Filtered Back Projection (FBP) for better digital breast tomosynthesis reconstruction," Proc. SPIE 6142, 122-130 (2006).

23. L. Zhou, J. Oldan, P. Fisher, and G. Gindi, “Low-contrast lesion detection in tomosynthetic breast imaging using a realistic breast phantom,” Proc. SPIE 6142, 1685-1696 (2006).
24. J. T. Rakowski and M. J. Dennis, “A comparison of reconstruction algorithms for C-arm mammography tomosynthesis,” Med. Phys. 33(8), 3018-3032 (2006).
25. M Bissonnette, M Hansroul, E Masson, S Savard, S Cadieux, P Warmoes, D Gravel, J Agopyan, B Polischuk, W Haerer, T Mertelmeier, J Lo, Y Chen, J Dobbins, J Jesneck, S Singh, “Digital breast tomosynthesis using an amorphous selenium flat panel detector,” *Proc. SPIE 5745, 529-540 (2005).*
26. J. T. Dobbins, III., “Matrix Inversion Tomosynthesis improvements in longitudinal x-ray slice imaging”, U.S. Patent #4,903,204 (1990). Assignee: Duke University.
27. Y. Chen, J. Y. Lo, J. T. Dobbins III, “Importance of point-by-point Back Projection (BP) correction for isocentric motion in digital breast tomosynthesis: relevance to morphology of microcalcifications,” submitted manuscript.
28. P. C. Bunch, “Comparison of signal-to-noise ratios for some new screen-film systems,” *Proc. SPIE 486, 99-107, (1984).*
29. P. C. Bunch, “Detective quantum efficiency of selected mammographic screen-film combinations,” *Proc. SPIE 1090, 67-77 (1989).*
30. J. M. Boone, T. R. fewell and R. J. Jennings, “Molybdenum, rhodium, and tungsten anode spectral models using interpolating polynomials with application to mammography,” *Med. Phys. 24 (12), 1863-1874 (1997).*
31. E. Samei, N. T. Ranger, J. T. Dobbins III, and Y. Chen, “Intercomparison of methods for image quality characterization: I. modulation transfer function,” *Med. Phys. 33 (5), 1454-1465 (2006).*
32. J. T. Dobbins III, E. Samei, N. T. Ranger, and Y. Chen, “Intercomparison of methods for image quality characterization: II. noise power spectrum,” *Med. Phys. 33 (5), 1466-1475 (2006).*